a v-Akt transformed lung epithelial cell line to wild type (11). TRB3 was also identified as a negative modulator of the PKB type (12), although a contradictory report was very recently published (13). These results indicate that understanding PKB modulation is important for elucidating the mechanism of PKB activation and its regulation of cellular functions.

In this study, we identified a novel protein that interacts with PKB (*in vivo* and *in vitro*). Without growth factor stimulation, overexpression of this protein markedly enhances phosphorylation of Thr^{308} and Ser^{473} in PKB, leading to its kinase activation and phosphorylation of its downstream substrates such as GSK-3 and FKHR. In addition, suppression of APE using RNA interference significantly reduces PKB phosphorylation and PKB kinase activity. Therefore, we termed this protein APE (Akt-phosphorylation enhancer) and herein demonstrate the possible role of APE in DNA synthesis and apoptosis in cooperation with PKB.

MATERIALS AND METHODS

Yeast Two-hybrid System—The DupLEX-A two-hybrid system (OriGene) was used for screening. We screened a mouse embryonic cDNA library with the pJG4-5 vector with a bait protein corresponding to the full length of mouse PKBα using a pEG202 vector and yeast strain EGY48. The positive clones were selected and assayed for β-galactosidase activity. Plasmid DNAs were isolated from positive clones and co-transformed with bait cDNA or negative control cDNA back into yeast to reconfirm the interaction. A yeast β-galactosidase assay kit (Pierce) was used to measure the protein-protein *in vivo* interaction according to the manufacturer's instructions.

Northern Blotting—Mouse Multiple Tissue Northern blot (Clontech) was used for Northern blotting. APE cDNA corresponding to the 600 bp of the coding region of the C-terminal and 400 bp of the untranslated region was used as a probe.

Antibody against APE—Fragments of the cDNA clone were subcloned into a glutathione *S*-transferase (GST) expression vector (Amersham Biosciences), expressed in BL21 and purified using glutathione-coupled Sepharose beads. Purified GST fusion proteins were injected into rabbits, and antisera were affinity-purified using the respective antigens. APE-C was generated to a fragment of APE encompassing amino acids 1646–1845. APE-N1 corresponded to amino acids 172–372, and APE-N3 to corresponded to 501–601. Polyclonal antibodies to each antigen were affinity-purified, using each GST fusion protein, after removal of GST-specific antibody.

Gene Constructions and Expression System in Yeast and Mammalian Cells—Full-length APE cDNAs were cloned into the pShuttle vector to express these proteins with an adenovirus expression system (Clontech). The expression cassette was excited and subcloned into pAdeno-X vector (Clontech). Adenovirus was cloned, and large scale virus purification from 293T cell lysates was achieved by performing CsCl density gradient centrifugation twice, followed by overnight dialysis as previously described. An adenovirus expression vector for PKBα with a Myc tag at its C terminus had previously been generated (14). PKBβ, the PKBα PH domain (residues 1–106), the PKBα kinase domain (residues 138–418), PKBα kinase and its hydrophobic domain (residues 148–480), and the PKBα hydrophobic domain (residues 418–480) were generated by PCR using PKBα or PKCβ cDNA as described previously (14). SGK1 (residues 98–431), SGK2 (residues 35–333), PKCβ2 (residues 342–673), and PKCε (residues 408–737) were generated by PCR using a mouse testis cDNA template. APE fragments were generated by PCR using full-length cDNAs as templates. The PCR products were cloned into pEG202 or pJG4-5 vectors.

Cell Cultures—HepG2, COS-7, and HeLa cells were from the RIKEN Cell Bank. Cells were maintained in Dulbecco's modified Eagle's medium supplemented with 10% fetal bovine serum under a 5% CO_2 atmosphere at 37 °C.

Immunoblot Analysis—The antibodies used in this study were anti-Myc (Upstate Biotechnology), anti-Akt, anti-phospho-Thr^{308}-Akt, anti-phospho-Ser^{473}-Akt, anti-phospho-Thr^{68}-Chk2, anti-phospho-Ser^{256}-FKHR, anti-phospho-$Ser^{20/9}$-GSK-3α/β, anti-caspase 3, anti-cleaved caspase 3, anti-poly(ADP-ribose) polymerase (PARP), anti-cleaved PARP (Cell Signaling Technology) anti-FLAG and anti-α tubulin (Sigma). For total cell lysates, cells were washed with ice-cold phosphate-buffered saline twice and collected with Laemmli sample buffer containing 100 mM dithiothreitol before separation by SDS-10% to 6% or 10% polyacrylamide gel. Proteins were transferred to nitrocellulose membranes. Immunoblotting was performed with ECL according to the manufacturer's instructions.

In Vivo Association of APE and PKB—HeLa cells were resuspended (4×10^7 cells/ml) in buffer A (10 mM HEPES (pH 7.9), 10 mM KCl, 1.5 mM $MgCl_2$, 0.34 M sucrose, 10% glycerol, 1 mM dithiothreitol, 5 μg/ml aprotinin, 5 μg/ml leupeptin, 0.5 μg/ml pepstatin A, 0.1 mM phenylmethylsulfonyl fluoride). Mouse testis was homogenized with 50 strokes, using a Teflon/glass homogenizer, in 10 volumes of ice-cold buffer A. Triton X-100 (0.1%) was added, and the cells were incubated for 5 min on ice. The supernatant was clarified by high speed centrifugation (15 min, 20,000 × *g*, 4 °C) to remove nuclei, cell debris, and insoluble aggregates. Endogenous PKB and APE in the HeLa cell lysate or mouse testis lysates were immunoprecipitated with 100 μg of immobilized anti-PKB and anti-APE-C antibodies, respectively. One hundred micrograms of immobilized Rabbit IgG were used as a control. The immunoprecipitates were washed four times in buffer A with 0.1% Triton X-100, eluted with elution buffer, electrophoresed, and transferred to nitrocellulose membranes. These filters were subjected to immunoblotting using the antibodies against APE and PKB.

In Vitro Association of APE and PKB—cDNAs encoding amino acids 418–480 of mouse PKBα with the Myc tag and amino acids 1646–1845 of mouse APE with the FLAG tag at their C termini were amplified by PCR. These cDNAs were cloned into pGEX-5X-1 and pET-28a vectors, and fusion protein expressions were induced in *E. coli* strain BL21 by the addition of 0.1 mM isopropyl β-D-thiogalactoside. The expressed proteins were purified using GST or His tag, according to the manufacturer's instructions. GST alone, GST-APE fragment fusion protein, and GST-PKB fragment fusion protein were incubated with glutathione-Sepharose 4B beads (Amersham Biosciences) for 3 h at 4 °C followed by extensive washing in NETN buffer (20 mM Tris-HCl, pH 8.0, 100 mM NaCl, 1 mM EDTA, 0.5% Nonidet P-40). An aliquot containing 20 μg of GST alone and GST-APE fragment fusion protein bound to beads were then incubated with the His tag PKB fragment. Similarly, an aliquot containing 20 μg of GST alone and the GST-PKB fragment fusion protein bound to beads were then incubated with the His tag APE fragment. After a 4-h incubation at 4 °C, the beads were washed five times with NETN buffer. The bound proteins were eluted by incubating the beads in SDS loading buffer containing 0.1 M dithiothreitol, electrophoresed, and then immunoblotted using anti-Myc and anti-FLAG antibodies for detection of the His tag PKB fragment and His tag APE fragment, respectively.

Immunoprecipitation and PKB Kinase Assay—Cells were lysed in Nonidet P-40 lysis buffer (50 mM Tris-HCl pH 7.5, 1% Nonidet P-40, 120 mM NaCl, 1 mM EDTA, 50 mM NaF, 40 mM β-glycerophosphate, 0.1 mM Na_3VO_4, 1 mM phenylmethylsulfonyl fluoride, 10 μg/ml aprotinin, 50 μg/ml leupeptin). For co-immunoprecipitation, we incubated protein lysates with primary antibodies overnight at 4 °C followed by incubation with Protein A-Sepharose. Immunoprecipitates were washed three times with Nonidet P-40 lysis buffer. An Akt kinase assay kit (Cell Signaling Technology) was used to measure PKB kinase activity. PKB was immunoprecipitated with anti-Myc antibody and Protein G-Sepharose. PKB kinase activity was detected using GSK-3β recombinant protein as a substrate according to the manufacturer's instructions.

Gene Transduction and in Vivo Phosphorylation of PKB—Mammalian cell lines were infected with adenovirus the day after plating. Purified virus was added directly to the culture medium. Titers of adenovirus for protein overexpression were adjusted so that the expression levels of the Myc-tagged PKBα were similar, irrespective of APE co-expression. Likewise, APE expression levels were adjusted so as to be similar, irrespective of Myc-tagged PKBα co-expression. Experiments were performed 36 h later for *in vivo* phosphorylation. Cells were starved for 12 h with KRB-Hepes buffer (118.5 mM NaCl, 4.7 mM KCl, 2.5 mM $CaCl_2$, 1.2 mM KH_2PO_3, 1.2 mM $MgSO_3$, 24.9 mM $NaHCO_3$, 30 mM HEPES, pH 7.4) containing 20 mg/ml bovine serum albumin. Cells were stimulated by the indicated stimulant in each experiment and, whenever indicated, 1 μM wortmannin or 10 μM LY294002 1 h prior to stimulation.

Gene Silencing by siRNA—Gene silencing was performed by an adenovirus-mediated siRNA method. For silencing of endogenous APE gene expression in HepG2 cells, a sense fragment (GGATCCGCATTA-ACACCCACCCGCTCTTCAAGAGAGAGCGGGTGGGTGTTAATGTT-TTTTCTAGAGAATTC) and an antisense fragment (GAATTCTCTAG-AAAAAACATTAACACCCACCCGCTCTCTCTTGAAGAGCGGGTGG-GTGTTAATGCGGATCC) were used for human APE. These two oligonucleotides were annealed *in vitro*, and the resultant double-stranded DNA fragments were subcloned into the BamHI-EcoRI site of a pSIREN-Shuttle vector. A negative control vector was supplied by Clontech. The expression cassette containing siRNA of APE or the negative control was excited and subcloned into pAdeno-X vector.

A

B

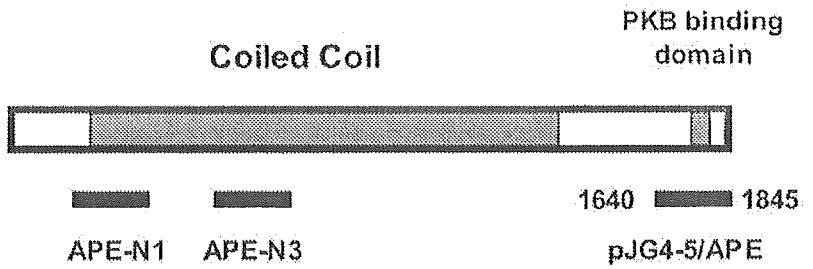

FIG. 1. **Structure and sequence of APE.** *A*, amino acid sequence of mouse APE. *B*, cDNA clones of APE isolated from the yeast two-hybrid screen and the fragments (APE-N1, APE-N3, and APE-C identical to pJG4–5/APE) used to generate an APE-specific antibody are shown *aligned below* a representation of full-length APE.

DNA Synthesis—HepG2 cells were maintained in Dulbecco's modified Eagle's medium supplemented with 10% fetal calf serum for 36 h and then transfected with an adenovirus encoding siRNA of APE or the negative control. Seventy-two hours after transfection, culture media were changed to Dulbecco's modified Eagle's medium supplemented with 0.2% bovine serum albumin, and cells were incubated for an additional 24 h. The cells were then incubated with BrdUrd labeling solution for 4 h. Incorporated BrdUrd was detected by cell proliferation ELISA, BrdUrd (colorimetric) (Roche Applied Science).

3-[4,5-Dimethylthiazol-2-yl]-2,5-diphenyltetrazolium Bromide (MTT) Assay—Cellular proliferation was measured by reduction of MTT, which corresponds to the living cell number and metabolic activity (15). Cells were plated at 5×10^4 cells/well in 24-well plates and transfected with adenovirus. After incubation for the indicated time, MTT solution was added to each well. After 1 h of incubation, the reaction was stopped by adding 1 ml of isopropyl alcohol with 0.04 N HCl. The absorbance of each well was measured at 492 and 630 nm using a microplate reader.

Cell Viability Analysis—HepG2 cells and HeLa cells were infected with control GFP, PKB, APE, or both PKB and APE adenoviruses and incubated for the indicated times. Floating cells were recovered from culture medium by centrifugation at $1200 \times g$ for 1 min, and adherent cells were harvested by trypsinization. Both the floating and adherent cells were observed for morphologic changes with a light microscope at ×200 magnification. We combined the adherent and floating cells and measured their viability by using a trypan blue dye exclusion assay.

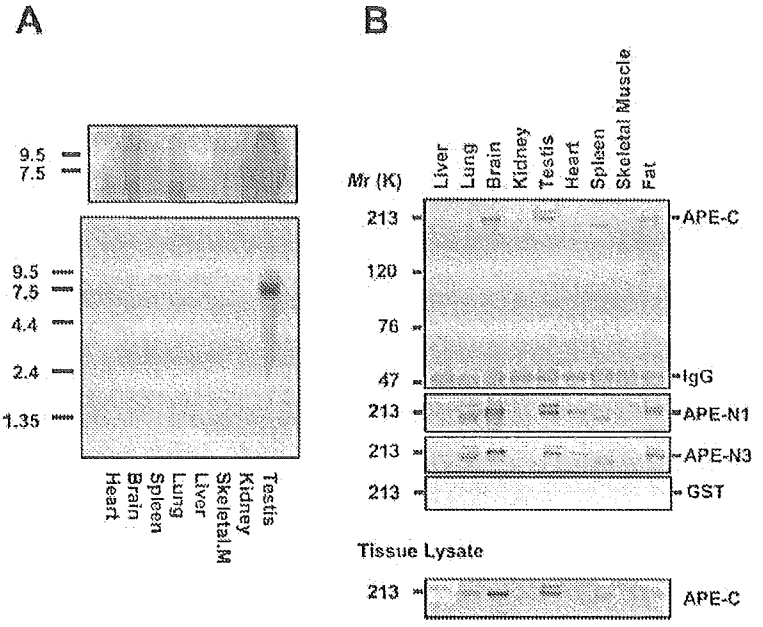

FIG. 2. **Tissue distribution of APE.** *A*, multiple tissue Northern (*MTN*; Clontech) blots probed with 3′ coding and untranslated region of APE. The *upper panel* represents the results of long exposure. *B*, Western analysis of APE. 50 μg of each tissue protein were immunoprecipitated with α-APE-C and immunoblotted with α-APE-C, α-APE-N1, α-APE-N3, and α-GST (*first* to *fourth panels*). Lysates of mouse tissues without immunoprecipitation were also used for immunoblotting with α-APE-C (*bottom panel*). The portions recognized by each antibody are shown under "Materials and Methods" and in Fig. 1.

Cell Cycle Analysis by Flow Cytometry—For cell cycle synchronization, cells were arrested at the G_1-S phase transition separated by two subsequent thymidine blocks (2 mM thymidine) for 14 h, separated by a period of 10 h without thymidine. Both adherent and nonadherent cells were harvested by trypsinization, and an aliquot of 2×10^6 cells was fixed in ice-cold ethanol for at least 1 h at 4 °C. The cells were collected by centrifugation and resuspended in propidium iodine (10 μg/ml) solution containing RNase for analysis of DNA content. Data were then collected on a BD Biosciences FACScan, 20,000 events/sample, using Cellquest software. DNA content analysis was performed with Verity ModFit software for the Macintosh computer.

RESULTS

Cloning of cDNAs Encoding the Protein Binding with PKB—Using full-length mouse PKB as bait in a yeast two-hybrid screen of an embryonic mouse complementary DNA library, we isolated 31 clones displaying β-galactosidase activity. Sequencing analysis revealed 10 of the clones with the strongest β-galactosidase activity to be identical. In all cases, 606 bp of the coding region were followed by a 3′-untranslated region. Isolation of the full-length cDNA by phage screening of the mouse embryonic cDNA library and a series of 5′ rapid amplifications of cDNA ends by PCR showed the largest open reading frame to be 5538 bp, which encode a 1845-amino acid protein with a predicted relative molecular mass (M_r) of 212,478 (Fig. 1*A*, accession number AB087827). By searching several data bases, we found that some mouse clones (BC037020, BC079895, AK129310) and this cDNA to be identical to a mouse homologue of the Kazusa DNA Research Institute clone KIAA1212. This clone is located on mouse chromosome 11 and on human chromosome 2. Although some cDNAs in the data base are presented as "full-length," it seems that they are not, judging from the size of the protein shown in this study. Our mouse cDNA is very likely to be full-length, and this protein was subsequently shown to enhance the phosphorylation of PKB, such that we designated the clone APE (Akt-phosphorylation enhancer). Protein analysis of APE revealed it to be a hydrophilic protein, and that its N terminus has a significant similarity with the putative coiled coil domain of the myosin heavy chain (Fig. 1*B*).

Tissue Distribution of APE—Northern blot analysis detected a 7.9-kb band of APE messenger RNA in the testis (Fig. 2*A*). Longer exposure revealed moderate expression in the brain, and low expressions in the spleen and lungs (Fig. 2*A*, *upper panel*). Anti-APE antibodies were generated against the three different portions of APE (Fig. 1*B*). Immunoblotting with antibodies against APE, irrespective of the differences in the

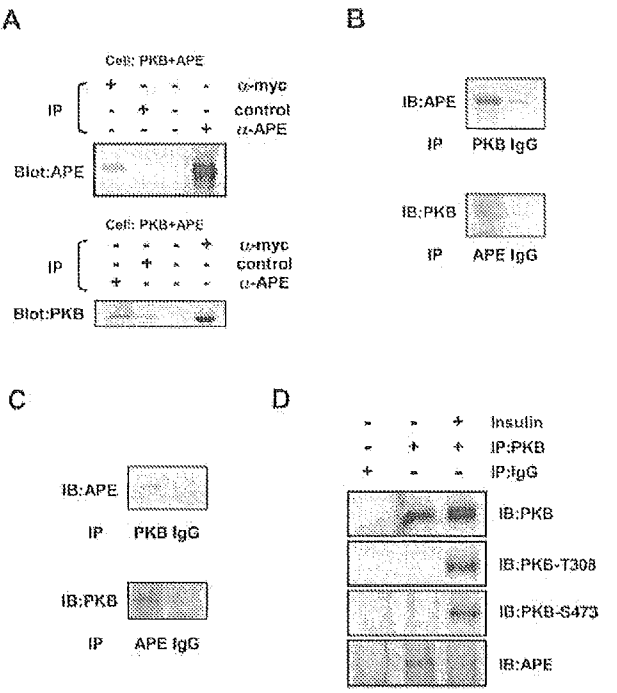

FIG. 3. **Interactions of APE with PKB *in vivo*.** *A*, binding of APE to Myc-PKB. Both APE and Myc-PKB were expressed in COS-7 cells. Immunoprecipitations (*IP*) from cell lysates were performed with the antibodies indicated on the *upper side* of *A*. Immunoblotting (*IB*) using anti-APE-C (*upper panel*) or anti-PKB (*lower panel*) is shown. APE was co-immunoprecipitated with PKB. Endogenous APE and PKB bind *in vivo*. HeLa cells (*B*) or mouse testes (*C*) were homogenized and immunoprecipitated with the antibody indicated *below* the *panels*. APE specifically immunoprecipitated with anti-PKB antibody, and PKB specifically immunoprecipitated with APE antibody. *D*, interaction of APE and PKB was inhibited after insulin stimulation. HEK293 cells were serum starved for 24 h and treated with 100 nM insulin for 15 min. Endogenous PKB were immunoprecipitated with α-PKB monoclonal antibody or with control IgG, and the amount of APE associated with PKB was analyzed by Western blotting.

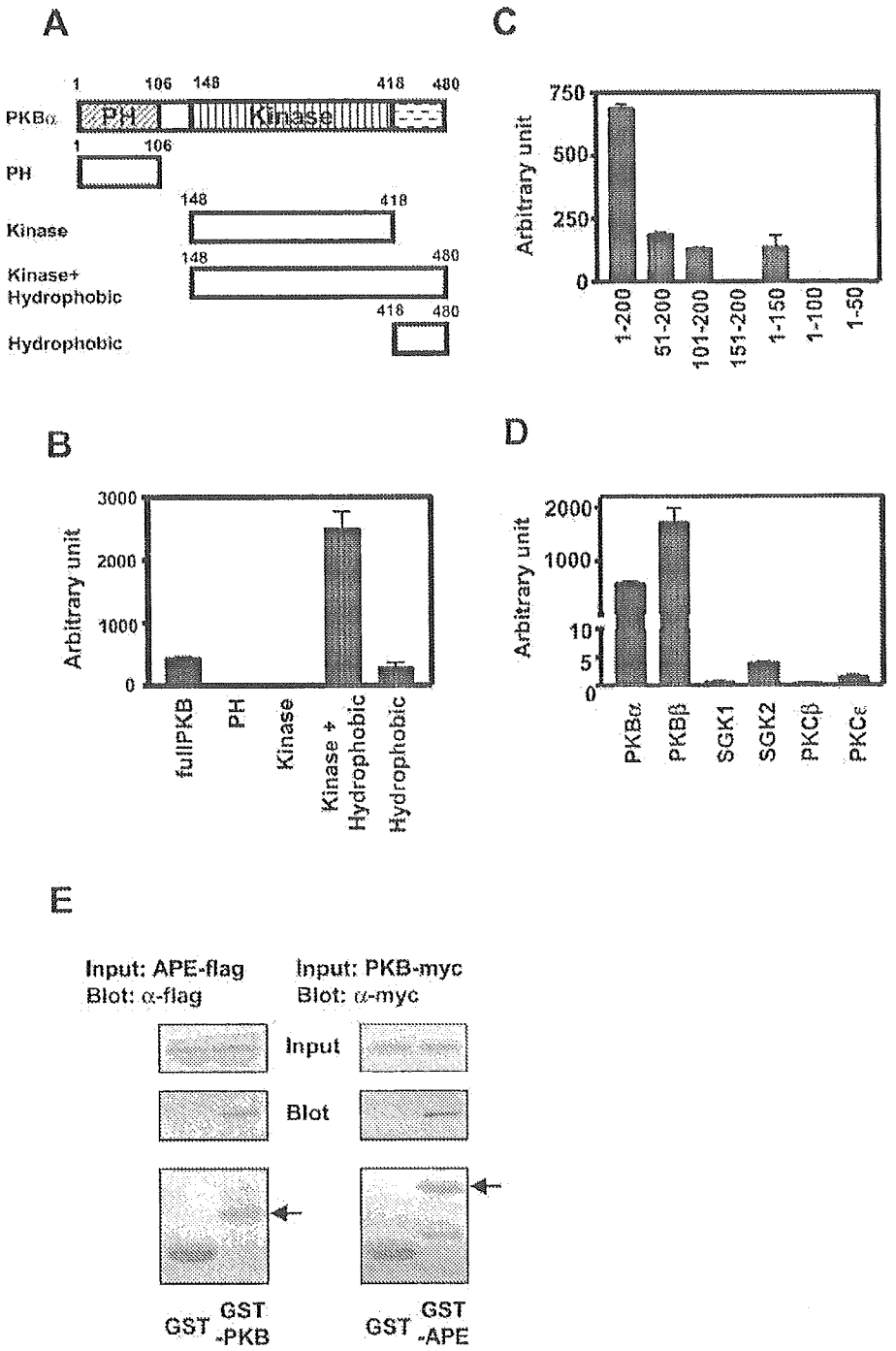

FIG. 4. **APE is a PKB-specific binding protein and has a domain responsible for the association.** *A*, PKBα structural domains and pEG202-PKBα fusion proteins. *B*, *in vivo* interaction of APE and PKBα structural domain. Interactions of APE-200 amino acids with PKBα, the PH domain, kinase domain, kinase domain with the hydrophobic domain, and the hydrophobic domain of PKBα are indicated as arbitrary units. *C*, *in vivo* interactions of PKBα and APE fragments. pEG202-PKBα was expressed in EGY48 with the indicated portion of the C-terminal of APE. β-Galactosidase activity is indicated as arbitrary units. *D*, *in vivo* interactions of APE and AGC kinases. pEG202-PKBα was expressed in EGY48 with PKBα, PKBβ, SGK1, SGK2, PKCβ, or PKCε. These *in vivo* interactions were measured by β-galactosidase activity. *E*, physical association of APE and PKB *in vitro*. Extracts from *E. coli* BL21 cells expressing PKBα or APE with a pET system were used to test for APE or PKBα binding to the following bead matrices: GST beads coupled to either bacterially expressed GST or GST-PKB (amino acids 418–480) or GST-APE (amino acids 1646–1845). Extract bead complexes were washed three times to remove weakly bound protein prior to eluting off specifically bound proteins. The pulled down APE (FLAG-tagged) and PKBα (Myc-tagged) were resolved on an SDS-polyacrylamide gel and detected by α-FLAG or α-Myc antibody.

epitopes of these antibodies (Fig. 1*B*), identified three bands of 220, 213, and 203 kDa in mouse tissues, whereas the control antibody against GST did not recognize any of these bands (Fig. 2*B*). The largest band of 220 kDa was observed in the lungs, testis, and fat. The 213-kDa band was detected in the brain, testis, heart, and fat. Finally, the smallest (203-kDa) band was detected in the lungs and spleen. These results were similarly obtained by immunoblotting of either immunoprecipitates of

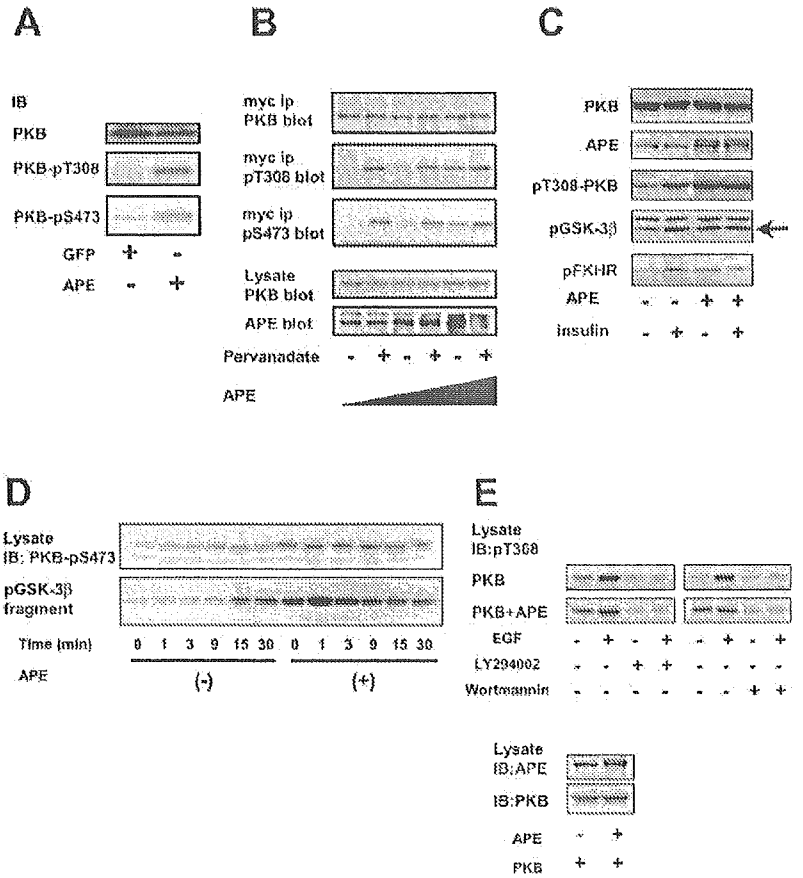

FIG. 5. **APE enhances basal PKB activity without growth factor stimulation.** *A*, basal phosphorylation of native PKB was enhanced by APE. COS-7 cells were transfected with GFP or APE and then serum-starved for 12 h. Basal phosphorylations of Thr^{308} and Ser^{473} were detected by specific antibodies. *IB*, immunoblot. *B*, APE enhances basal PKB phosphorylation without pervanadate stimulation. COS-7 cells were co-transfected with Myc-PKBα and with increasing amounts of APE. Cells were next serum-starved for 12 h and then stimulated with vehicle or 100 μM pervanadate for 15 min at 37 °C. Cell lysates were next immunoprecipitated with Myc antibody, and the phosphorylation states of Thr^{308} and Ser^{473} were determined by specific antibodies. *C*, APE enhances downstream PKBα without insulin stimulation. HepG2 cells were transfected with Myc-PKBα and with or without APE, as indicated in *C*. Cells were serum-starved for 12 h and then stimulated with 10^{-7} M insulin for 15 min. Phosphorylations of Ser^{9} of GSK-3β and Ser^{256} of FKHR were detected by specific antibodies. *D*, APE enhanced PKB kinase activity without pervanadate stimulation. Myc-PKBα was transfected into COS-7 cells in the presence or absence of APE, as indicated. Cells were serum-starved and then stimulated with vehicle control or 100 μM pervanadate for the indicated times. Myc-PKB was immunoprecipitated, and phosphorylation of Ser^{473} of PKB was detected by a specific antibody. An *in vitro* kinase assay was performed using a GSK-3β fragment as the substrate for PKB kinase, and kinase activity was determined using the GSK-3β phospho-Ser^{9} antibody. *E*, APE-induced basal phosphorylation of PKBα was inhibited by LY294002 and wortmannin. COS-7 cells were transfected with Myc-PKBα, with or without APE. Cells were serum-starved for 12 h and then stimulated with 50 μM epidermal growth factor for 15 min. The cells were incubated with 10 μM LY294002 or 1 μM wortmannin for 1 h prior to epidermal growth factor stimulation.

tissue lysates (Fig. 2*B*, *upper panel*) or nonimmunoprecipitated lysate (Fig. 2*B*, *lower panel*). These results suggest the existence of alternatively spliced protein products from the APE gene because a search of human expressed sequence tag databases indicated the existence of alternatively spliced forms of APE (data not shown).

In Vivo Association of PKB and APE—Next, to demonstrate *in vivo* association between APE and PKB, full-length APE and c-Myc-tagged PKBα were overexpressed in COS-7 cells. As shown in the *upper panel* of Fig. 3*A*, APE was detected in the immunoprecipitate by the anti-Myc antibody (Fig. 3*A*, *upper panel*). Similarly, PKB was detected in the anti-APE immunoprecipitate (Fig. 3*A*, *lower panel*). This interaction between APE and PKB was demonstrated when both were overexpressed in Sf-9 insect cells or HepG2 cells (data not shown).

We also demonstrated an endogenous interaction between PKB and APE by coimmunoprecipitation of the endogenous proteins using specific antibodies in HeLa cells, and mouse testis. As shown in Fig. 3*B*, APE was coimmunoprecipitated by anti-PKB antibody in HeLa cells. PKB was also coimmunoprecipitated by anti-APE-C antibody as shown in the *lower panel*. The PKB and APE interaction was reconfirmed by the same procedure using mouse testis homogenates (Fig. 3*C*), indicating that the PKB-APE interaction occurs under physiological conditions.

APE Binds to Nonphosphorylated PKB More Efficiently than Phosphorylated PKB—The effect of PKB phosphorylation on the interaction between APE and PKB was assessed by measuring the amount of APE co-immunoprecipitated with PKB in the presence and absence of insulin stimulation (Fig. 3*D*). Insulin stimulation induced the phosphorylation of PKB on Thr^{308} and Ser^{473}. The amount of APE co-immunoprecipitated with PKB was revealed to be significantly lower in the insulin-stimulated condition, compared with the unstimulated condition (Fig. 3*D*, *bottom panel*). This result suggests that APE has a higher affinity for nonphosphorylated than for phosphorylated PKB.

APE Binds to the C-terminal Portion of PKB but Not to Other AGC Kinases—To determine the region of PKB responsible for binding with APE, we generated four deletion mutants consist-

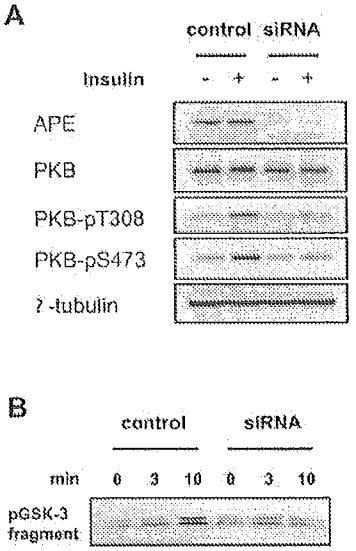

FIG. 6. **APE siRNA reduced insulin-stimulated endogenous PKB phosphorylation and kinase activity in HepG2 cells.** HepG2 cells were transfected with adenovirus expressing negative control siRNA or APE siRNA for 60 h, starved for 12 h, and treated with 100 nM insulin for 15 min. *A*, endogenous PKB were immunoprecipitated with α-PKB monoclonal antibody, and PKB phosphorylation was analyzed by Western blotting using phosphospecific antibodies of Thr^{308} or Ser^{473}. PKB and APE expression levels were analyzed using cell extracts. *B*, endogenous PKB immunoprecipitated by α-PKB monoclonal antibody from control or APE-depleted HepG2 cells was also used for an *in vitro* kinase assay.

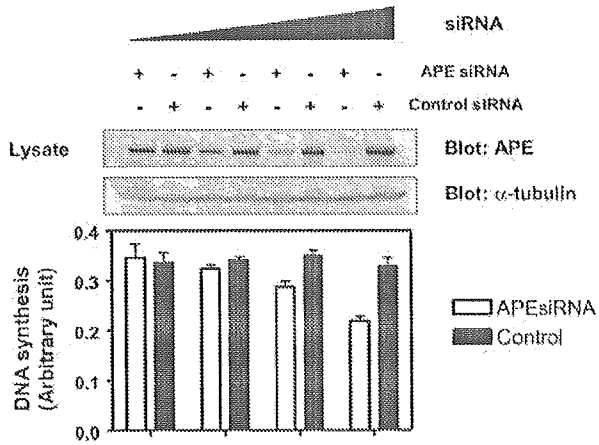

FIG. 7. **Phosphorylation of PKB and DNA synthesis were reduced by knockdown of APE.** HepG2 cells were transfected with adenovirus expressing negative control siRNA or APE siRNA. DNA synthesis in cells cultured in Dulbecco's modified Eagle's medium supplemented with 0.2% bovine serum albumin was measured by BrdUrd incorporation.

ing of a PH domain, kinase domain, kinase and hydrophobic domain, or the hydrophobic domain in the carboxyl terminus of PKB (16) (Fig. 4*A*). These mutants were subjected to baits in a yeast two hybrid screening with APE. It was revealed that the kinase domain with the hydrophobic motif or the hydrophobic motif alone binds with APE, whereas neither PH nor the kinase domain can bind with APE (Fig. 4*B*).

Subsequently, several deletion mutants of APE were produced to determine the portion responsible for the association with PKB. The C-terminal portion was shown to consist of 200 amino acids of APE, sufficient for the association with PKB. Since the deletion mutant amino acids 101–200 or 1–150 retain the ability to bind PKB, it is likely that the minimal portion necessary for the association with PKB is located within amino acid sequence 101–150 (Fig. 4*C*).

PKB belongs to a family of protein kinases, originally including protein kinase A, cGMP-dependent protein kinase and protein kinase C, termed the AGC family. Proteins in this family contain regions of high homology in their kinase domains (1). Since AGC kinases contain regions of high homology with the hydrophobic motif in PKB, we further examined whether APE interacted with AGC kinases other than PKB, using a yeast two-hybrid system. SGK1, SGK2, PKCβ2, PKCε, and PKBβ/Akt2 have a kinase domain and a hydrophobic motif highly homologous to those of PKBα. As a result, PKBβ and PKBα bind efficiently to APE in yeast (Fig. 4*D*). Conversely, very little interaction with APE was observed for SGK1, SGK2, PKCβ2, or PKCε. These results indicate that APE is not a common AGC kinase-binding protein but, rather, a PKB-specific binding protein.

In Vitro Association between Amino Acids 418–480 of PKB and Amino Acids 1646–1845 of APE—To examine whether the association of APE and PKB occurs *in vitro*, amino acids 418–480 of PKB and 1646–1845 of APE were expressed using *E. coli* and then purified. As shown in the *left panel* of Fig. 4*E*, GST-amino acids 418–480 of mouse PKBα fusion protein bound to His-tagged amino acids 1646–1845 of mouse APE protein, whereas GST alone did not. Similarly, GST-amino acids 1646–1845 of mouse APE fusion protein, but not GST alone, bound to His-tagged amino acids 418–480 of mouse PKBα (Fig. 4*E*, *right panel*). These results indicate that the interaction between APE and PKB is direct.

APE Markedly Enhances Basal Phosphorylation of PKB—PKBα is activated via phosphorylation of Thr^{308} in the activation loop of the kinase domain and of Ser^{473} in the hydrophobic motif of the carboxyl terminus (17–21). To test the effect of APE binding on phosphorylation of PKB, basal phosphorylation of endogenous PKBα in COS-7 cells transfected with GFP adenovirus or APE adenovirus was analyzed. As shown in Fig. 5*A*, there was no significant phosphorylation on Thr^{308} or Ser^{473} of PKBα after 12-h serum starvation (*left lane* of Fig. 5*A*), but Thr^{308} and Ser^{473} of endogenous PKB were apparently phosphorylated in cells overexpressing APE. A similar result was obtained for HepG2 cells (data not shown).

Pretreatment with pervanadate increased PKB phosphorylation, time-dependently, as reported previously (11). To explore the effect of APE on enhanced PKBα phosphorylation, we treated COS-7 cells with adenoviruses expressing PKBα and various amounts of APE. APE overexpression increased PKB phosphorylation, in a titer-dependent manner, and the maximal phosphorylation of PKB obtained by APE overexpression was comparable with that achieved by long term pervanadate stimulation (Fig. 5*B*). These results suggest that APE overexpression can induce essentially maximal phosphorylation of PKB on Thr^{308} and Ser^{473}, which indicates that APE is an enhancer of PKB *in vivo*.

Phosphorylation of PKB by APE Induces the Phosphorylation of GSK-3α/β and FKHR—PKB reportedly phosphorylates several downstream molecules such as GSK-3α/β and FKHR (17, 22). As a positive control, we confirmed that insulin stimulation induced PKB phsphorylation as well as downstream phosphorylation of Ser^{256} of FKHR and Ser^{9} of GSK-3β in HepG2 cells. Then we examined whether PKB phosphorylated by the overexpressed APE can induce the phosphorylations of GSK-3β and FKHR without growth factor stimulation. As shown in the right two lanes of Fig. 5*C*, overexpressed APE markedly enhanced phosphorylation of Ser^{256} of FKHR and Ser^{9} of GSK-3β, to degrees similar to those seen with insulin stimulation.

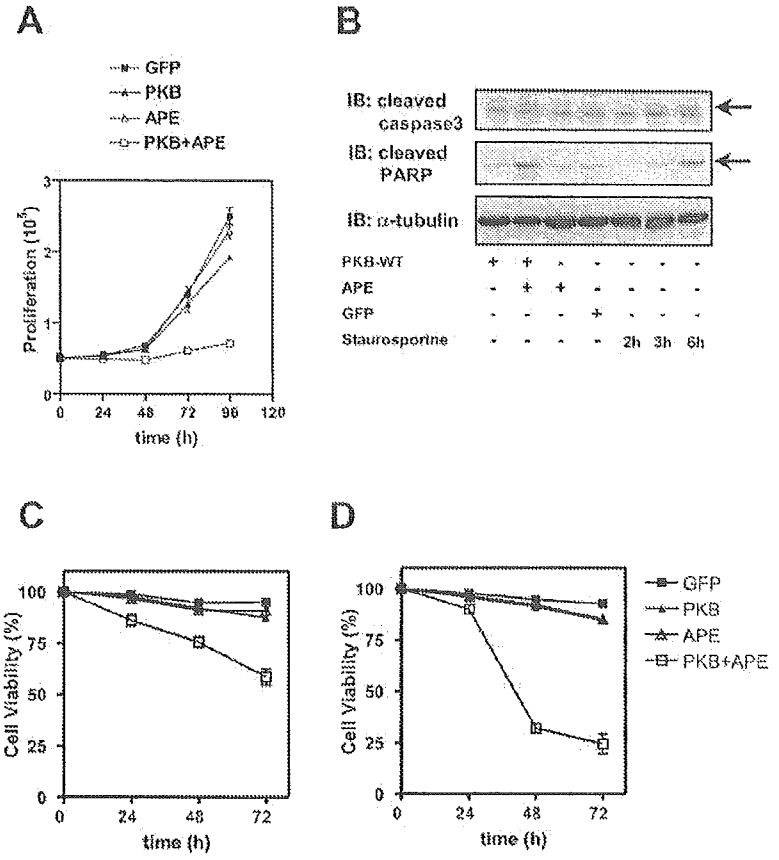

FIG. 8. **Inhibition of cell proliferation and induction of apoptosis by APE.** *A*, overexpressions of PKB and APE inhibited cell growth. COS-7 cells were transfected with adenoviruses encoding GFP, PKBα, APE, or PKBα with APE. At the indicated time after transfection, MTT assays were performed to measure cell growth. *B*, PKB and APE induce caspase-3 and PARP cleavage. COS-7 cells were either uninfected or infected with adenoviruses encoding GFP, PKBα, APE, or PKBα plus APE, for 36 h. The uninfected cells were treated with 500 ng/ml staurosporine for the indicated time prior to harvest. Cells were lysed and separated by SDS-PAGE and Western blotted (*IB*) with the indicated antibodies, shown on the *left*. *C* and *D*, overexpression of PKB and APE reduced cell viability. COS-7 cells (*C*) and HepG2 cells (*D*) were transfected with adenovirus encoding GFP, PKBα, APE, and PKBα with APE. Cell viability was measured by trypan blue dye exclusion assay.

In Vitro Kinase Activity of PKB Enhanced by APE—To test the influence of APE binding on PKB kinase activity, we assayed kinase activity in immune complexes from transfected COS-7 cells treated with pervanadate. Pervanadate-stimulated PKB activity was time-dependently increased when COS-7 cells were transfected with PKB alone, and kinase activity paralleled the phosphorylations of Thr^{308} and Ser^{473}. APE enhanced the basal phosphorylations of Thr^{308} and Ser^{473}, and *in vitro* kinase activity was also maximally enhanced and paralleled these phosphorylations. These results indicate that APE induces maximal basal phosphorylation of PKB, thereby maximally enhancing its kinase activity (Fig. 5*D*).

PI 3-Kinase Activity Is Needed for APE-induced PKB Phosphorylation—To examine whether the APE-induced increase in PKB phosphorylation is mediated only by PI 3-kinase, we examined the effects of the PI 3-kinase specific inhibitors LY294002 and wortmannin on APE-induced PKB phosphorylation. As shown in Fig. 5*E*, both epidermal growth factor-induced and APE-induced phosphorylation of PKB were completely inhibited by LY294002 and wortmannin treatments. These results indicate PI 3-kinase activity to be essential for APE-induced phosphorylation of PKB.

APE siRNA Inhibits Insulin-stimulated PKB Phosphorylation and Activation—To verify the role of endogenous APE in PKB phosphorylation, HepG2 cells were transfected with the negative control or small interfering RNA (siRNA) mediated by the adenoviral expression system. Suppression of endogenous APE by APE siRNA overexpression markedly reduced the APE protein level (Fig. 6*A*, *upper panel*). Under these conditions, endogenous PKB phosphorylation of both Thr^{308} and Ser^{473} in response to insulin was apparently reduced (Fig. 6*A*, *third* and *fourth panels*). Consistent with the PKB phosphorylation results, insulin-induced PKB kinase activity measured by *in vivo* kinase assay was also reduced in APE-deficient cells (Fig. 6*B*).

Knockdown of APE Reduces DNA Synthesis—To explore the effect of APE depletion on proliferation, DNA synthesis in HepG2 cells were measured by BrdUrd incorporation. It was shown that suppressed expression of endogenous APE by siRNA led to decreased DNA synthesis in an APE siRNA titer-dependent manner (Fig. 7).

Cell Death Induced by Overexpression of Both APE and PKB—Recent investigations have shown that overexpression of constitutively activated PKB mutants in many cell types promotes cellular proliferation and inhibits apoptosis (23–25). On the contrary, several lines of evidence indicate that down-regulation of PI 3-kinase/PKB is required to execute the mitotic program efficiently (26). To explore the effect of prolonged PKB activation induced by APE, we next analyzed the effect of APE on cellular proliferation using COS-7 cells (Fig. 8*A*). The expression of GFP protein by adenovirus had no effect on COS-7 proliferation. COS-7 cells expressing PKBα proliferated slightly more slowly than the control GFP-expressing cells. However, COS-7 cells expressing both PKBα and APE showed essentially no proliferation. Trypan blue exclusion was employed to assay cell viability in COS-7 cells and HepG2 cells overexpressing PKB and APE. COS-7 cells expressing both PKBα and APE showed reduced viability (*i.e.* these cells ultimately died) (Fig. 8*C*). Virtually the same observations were made in HepG2 cells (Fig. 8*D*).

Induction of Apoptosis by Overexpression of Both APE and PKB—To elucidate whether apoptosis is involved in the molecular mechanism of APE-induced inhibition of cellular proliferation and cell death, we analyzed the cleavage of caspase-3 and PARP (Fig. 8*B*). Caspase-3 and PARP are key mediators of apoptosis, and cleavage of these enzymes to their active form correlates with the onset of apoptosis (27, 28). When COS-7

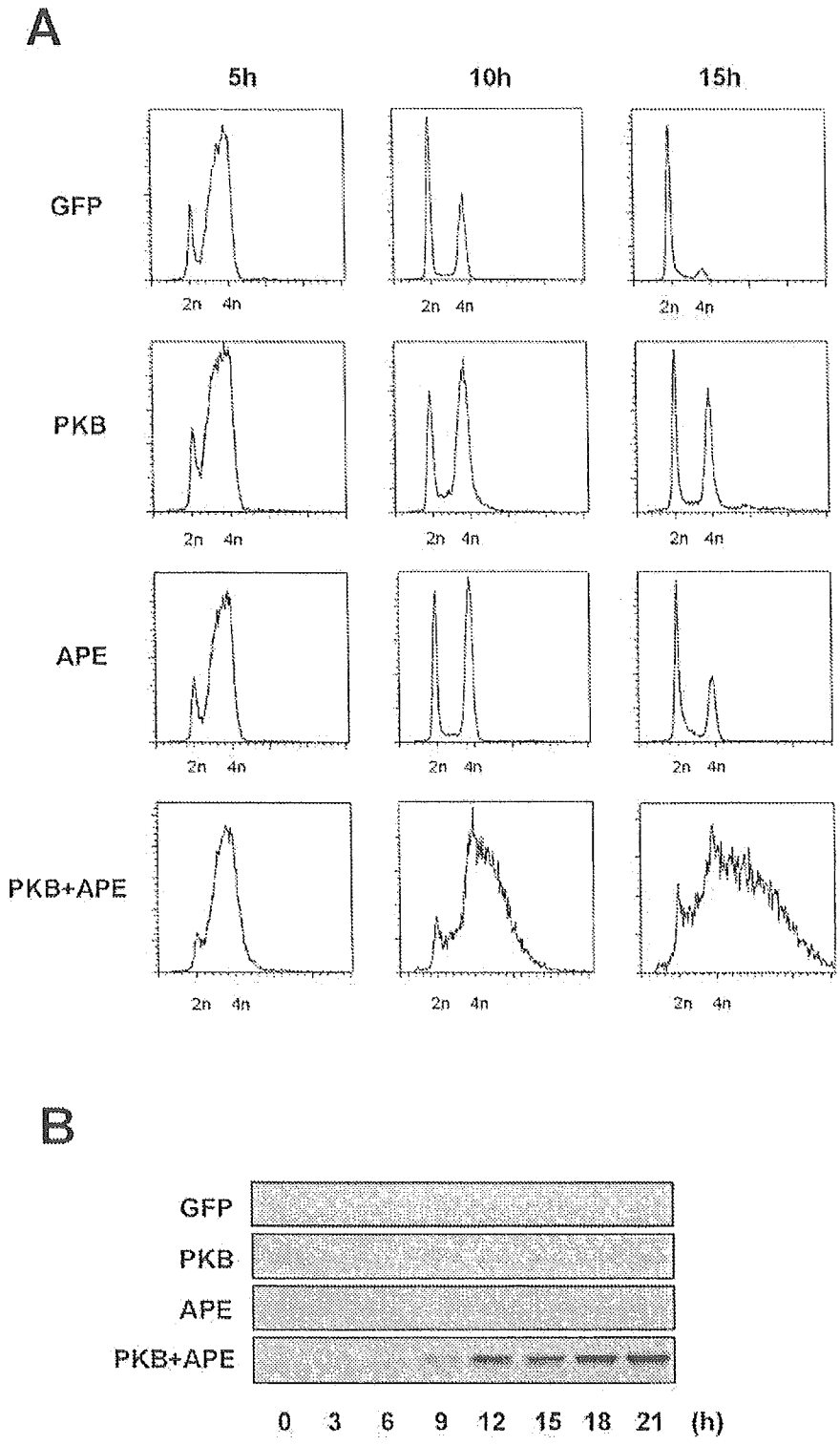

FIG. 9. **Overexpressions of PKBα and APE result in cells with greater than 4n DNA content.** *A*, APE and PKB, alone or in combination, were expressed with an adenovirus expression system, 18 h prior to thymidine release. Cells were collected at the indicated time points after thymidine release. As a control, cells expressing GFP were used. The DNA content was analyzed by fluorescence-activated cell sorting analysis. *2n* (diploid) and *4n* (tetraploid) represent the cells containing 2n and 4n DNA content, respectively. *B*, APE plus PKBα induces phosphorylation of Thr^{68} of Chk2. HeLa cells arrested in G_1/S by a double-thymidine method were released into a synchronous cell cycle and sampled every 3 h. Phosphorylation of Chk2 was determined by immunoblotting with a specific antibody for phospho-Thr^{68} of Chk2.

cells were treated with 1 μM staurosporine, cleaved caspase-3 and cleaved PARP were detectable after 3–6 h, in a time-dependent manner. In COS-7 cells expressing GFP, PKBα, or APE, using an adenovirus expression system, no cleavage of caspase-3 or PARP was detectable. However, in cells expressing both PKBα and APE, cleaved caspase-3 and PARP were

detected. These findings indicate that apoptosis is not induced by PKB alone but rather by the interaction between PKB and APE accompanying prolonged activation of PKBα.

Effect of APE-PKB Interaction on the Cell Cycle—To study the effect of the APE-PKB interaction on cell cycle progression, cell cycle profiles were analyzed using flow cytometry (Fig. 9*A*). Overexpression of PKB or APE alone did not promote rereplication. However, co-expression of PKB and APE generated cells that had DNA contents greater than normal G_2/M cells from 5 to 15 h after thymidine release, indicating that PKB and APE interact to induce DNA rereplication without mitosis.

APE-PKB Interaction Induces Chk2 Phosphorylation—Rereplication reportedly leads to DNA damage, and Vaziri *et al.* (29) demonstrated Chk2 phosphorylation in mammalian cells in which rereplication had been induced by overexpression of the replication license factors CDT1 and CDC6. The amount of Chk2 protein was not altered by PKBα or APE expression (data not shown). However, in HeLa cells overexpressing both PKBα and APE, Chk2 was apparently phosphorylated starting 6 h after thymidine block release, and peak phosphorylation was observed 12–21 h thereafter (Fig. 9*B*). In contrast, overexpression of neither PKBα nor APE induced apparent Chk2 phosphorylation.

DISCUSSION

In this study, we identified a novel PKB-binding protein using a yeast two-hybrid screening system and named it APE. The APE protein was detectable in many tissues including the brain, spleen, lung, fat, and heart, although APE mRNA was most abundant in the testis. In addition, from the immunoblotting results obtained using antibodies against different portions of APE, the presence of alternatively spliced protein products is likely.

The *in vivo* interaction of APE with PKB was clearly demonstrated by the overexpression of both proteins as well as by coimmunoprecipitation of the endogenous proteins. *In vitro* association was also demonstrated using bacterially expressed recombinant proteins. Notably, APE did not interact with any of the other AGC kinases tested in this study such as SGK1/2, PKCβ2, and PKCϵ, which have regions highly homologous to the hydrophobic motif of PKB. Thus, it is reasonable to consider APE a PKB-specific binding protein.

Subsequently, by overexpressing APE, we demonstrated that this protein markedly enhances the phosphorylation and kinase activity of PKB, whereas reducing endogenous APE expression using siRNA suppressed both. In addition, although APE binds to both phosphorylated and nonphosphorylated PKB, it seems that more PKB binds to APE when PKB is nonphosphorylated. Taking into consideration that APE-induced phosphorylation of PKB did not occur in cells treated with wortmannin or LY294002, APE itself is not a kinase and it is likely that APE enhances or prolongs the PI 3-kinase-dependent phosphorylation of PKB. In other words, we speculate that APE functions as a scaffold protein and facilitates Thr^{308} and Ser^{473} phosphorylation of PKB by PDK1/2. Alternatively, the APE·PKB complex may inhibit access of serine/threonine phosphatases such as protein phosphatase 2A.

Recent evidence indicates that PI 3-kinase and PKB play important roles in regulating cell proliferation. In this study, it was demonstrated that suppression of APE by siRNA reduced DNA synthesis, with decreased phosphorylation and kinase activity of PKB. This result agrees with those of previous reports showing the important role of PKB in proliferation. Thus, when the level of PKB expression is limited, APE apparently enhances proliferation in cooperation with PKB.

On the other hand, interestingly, we demonstrated overexpressions of both APE and PKB to induce DNA rereplication rather than normal DNA synthesis, thereby proving that these overexpressions together increase the cellular DNA content more than 4n in the S phase within 10 h after initiation of the S phase. Similar rereplication was reported with overexpression of the DNA replication factors Cdt1 and Cdc6 in either yeast or mammalian cells (29). In such cell systems, rereplication induced DNA damage, and the checkpoint pathway including Chk2 was activated. Chk2 activation is involved in the p53-dependent apoptotic response observed with DNA damage (30). In good agreement with these previous reports, we observed Chk2 phosphorylation and subsequent apoptosis in PKB and APE-expressing cells, after DNA rereplication. Thus, although the overexpression of both APE and PKB observed in this study may not be physiological, it is likely that the prolonged PKB phosphorylation induced by the association with APE does not lead to normal cell proliferation but rather to rereplication and the ensuing apoptosis. In other words, in the cells with high PKB expression, increased APE expression could lead to apoptosis after DNA rereplication.

Although we cannot explain how PKB and APE induce rereplication in human cells, we observed APE-induced PKB phosphorylation to be markedly enhanced not only in the cytoplasm but also the nucleus (data not shown). Thus, we speculate that overexpressed PKB and APE might phosphorylate some unidentified proteins in the nucleus such that normal replication licensing is blunted. However, this phenomenon was observed only with the overexpression system, and further study is needed to clarify whether this phenomenon is physiological.

In summary, we identified a novel PKB-binding protein, which enhances the phosphorylation of PKB and termed it APE. APE plays a role in regulating the phosphorylation state of PKB and the resultant DNA synthesis. In addition, DNA rereplication and the resultant apoptosis might be a novel mechanism that is induced by the enhanced interaction between APE and PKB, the physiological significance of which merits further investigation.

Acknowledgments—We thank K. Shibata and M. Hirano-Koyanagi for helpful discussions and technical assistance; T. Sugano, T. Kobayashi, M. Mimura, Y. Ito, and other laboratory members for technical assistance and K. Honjo for secretarial assistance.

REFERENCES

1. Lawlor, M. A., and Alessi, D. R. (2001) *J. Cell Sci.* **114,** 2903–2910
2. Datta, S. R., Brunet, A., and Greenberg, M. E. (1999) *Genes Dev.* **13,** 2905–2927
3. Walker, K. S., Deak, M., Paterson, A., Hudson, K., Cohen, P., and Alessi, D. R. (1998) *Biochem. J.* **331,** 299–308
4. Alessi, D. R., Caudwell, F. B., Andjelkovic, M., Hemmings, B. A., and Cohen, P. (1996) *FEBS Lett.* **399,** 333–338
5. Zhou, B. P., Liao, Y., Xia, W., Zou, Y., Spohn, B., and Hung, M. C. (2001) *Nat. Cell Biol.* **3,** 973–982
6. Zhou, B. P., Liao, Y., Xia, W., Spohn, B., Lee, M. H., and Hung, M. C. (2001) *Nat. Cell Biol.* **3,** 245–252
7. Inoki, K., Li, Y., Zhu, T., Wu, J., and Guan, K. L. (2002) *Nat. Cell Biol.* **4,** 648–657
8. Potter, C. J., Pedraza, L. G., and Xu, T. (2002) *Nat. Cell Biol.* **4,** 658–665
9. Pekarsky, Y., Koval, A., Hallas, C., Bichi, R., Tresini, M., Malstrom, S., Russo, G., Tsichlis, P., and Croce, C. M. (2000) *Proc. Natl. Acad. Sci. U. S. A.* **97,** 3028–3033
10. Basso, A. D., Solit, D. B., Chiosis, G., Giri, B., Tsichlis, P., and Rosen, N. (2002) *J. Biol. Chem.* **277,** 39858–39866
11. Maira, S. M., Galetic, I., Brazil, D. P., Kaech, S., Ingley, E., Thelen, M., and Hemmings, B. A. (2001) *Science* **294,** 374–380
12. Du, K., Herzig, S., Kulkarni, R. N., and Montminy, M. (2003) *Science* **300,** 1574–1577
13. Iynedjian, P. B. (2004) *Biochem. J.* **386,** 113–118
14. Yamada, T., Katagiri, H., Asano, T., Inukai, K., Tsuru, M., Kodama, T., Kikuchi, M., and Oka, Y. (2001) *J. Biol. Chem.* **276,** 5339–5345
15. Kamikubo, Y., Takaori-Kondo, A., Uchiyama, T., and Hori, T. (2003) *J. Biol. Chem.* **278,** 17609–17614
16. Downward, J. (1998) *Curr. Opin. Cell Biol.* **10,** 262–267
17. Cross, D. A., Alessi, D. R., Cohen, P., Andjelkovich, M., and Hemmings, B. A. (1995) *Nature* **378,** 785–789
18. Andjelkovic, M., Alessi, D. R., Meier, R., Fernandez, A., Lamb, N. J., Frech, M., Cron, P., Cohen, P., Lucocq, J. M., and Hemmings, B. A. (1997) *J. Biol. Chem.* **272,** 31515–31524
19. Alessi, D. R., Andjelkovic, M., Caudwell, B., Cron, P., Morrice, N., Cohen, P., and Hemmings, B. A. (1996) *EMBO J.* **15,** 6541–6551

20. Stokoe, D., Stephens, L. R., Copeland, T., Gaffney, P. R., Reese, C. B., Painter, G. F., Holmes, A. B., McCormick, F., and Hawkins, P. T. (1997) *Science* **277,** 567–570
21. Stephens, L., Anderson, K., Stokoe, D., Erdjument-Bromage, H., Painter, G. F., Holmes, A. B., Gaffney, P. R., Reese, C. B., McCormick, F., Tempst, P., Coadwell, J., and Hawkins, P. T. (1998) *Science* **279,** 710–714
22. Nakae, J., Park, B. C., and Accili, D. (1999) *J. Biol. Chem.* **274,** 15982–15985
23. Klippel, A., Escobedo, M. A., Wachowicz, M. S., Apell, G., Brown, T. W., Giedlin, M. A., Kavanaugh, W. M., and Williams, L. T. (1998) *Mol. Cell. Biol.* **18,** 5699–5711
24. Kops, G. J., Medema, R. H., Glassford, J., Essers, M. A., Dijkers, P. F., Coffer, P. J., Lam, E. W., and Burgering, B. M. (2002) *Mol. Cell. Biol.* **22,** 2025–2036
25. Dudek, H., Datta, S. R., Franke, T. F., Birnbaum, M. J., Yao, R., Cooper, G. M., Segal, R. A., Kaplan, D. R., and Greenberg, M. E. (1997) *Science* **275,** 661–665
26. Alvarez, B., Martinez, A. C., Burgering, B. M., and Carrera, A. C. (2001) *Nature* **413,** 744–747
27. Oliver, F. J., de la Rubia, G., Rolli, V., Ruiz-Ruiz, M. C., de Murcia, G., and Murcia, J. M. (1998) *J. Biol. Chem.* **273,** 33533–33539
28. Nicholson, D. W., Ali, A., Thornberry, N. A., Vaillancourt, J. P., Ding, C. K., Gallant, M., Gareau, Y., Griffin, P. R., Labelle, M., Lazebnik, Y. A., Munday, N. A., Raju, S. M., Smulson, M. E., Yamin, T. T., Yu, V. L., and Miller, D. K. (1995) *Nature* **376,** 37–43
29. Vaziri, C., Saxena, S., Jeon, Y., Lee, C., Murata, K., Machida, Y., Wagle, N., Hwang, D. S., and Dutta, A. (2003) *Mol. Cell* **11,** 997–1008
30. Jack, M. T., Woo, R. A., Hirao, A., Cheung, A., Mak, T. W., and Lee, P. W. (2002) *Proc. Natl. Acad. Sci. U. S. A.* **99,** 9825–9829

Available online at www.sciencedirect.com
SCIENCE DIRECT®
Diabetes Research and Clinical Practice 69 (2005) 287–292
DIABETES RESEARCH AND CLINICAL PRACTICE
www.elsevier.com/locate/diabres

WRN gene 1367 Arg allele protects against development of type 2 diabetes mellitus

Masashi Hirai [a,*], Susumu Suzuki [a], Yoshinori Hinokio [a], Takahiro Yamada [a], Shinsuke Yoshizumi [a], Chitose Suzuki [a], Jo Satoh [b], Yoshitomo Oka [a]

[a] *Division of Molecular Metabolism and Diabetes, Department of Internal Medicine, Tohoku University Graduate School of Medicine, 2-1 Seiryo-machi, Aoba-ku, Sendai 980-8575, Japan*
[b] *Department of Diabetology and Metabolism, Iwate Medical University, Japan*

Received 10 August 2004; received in revised form 14 January 2005; accepted 28 January 2005
Available online 16 March 2005

Abstract

Werner's syndrome is an autosomal recessive disease caused by mutation of the *WRN* gene, which may lead to DNA repair failure and acceleration of aging. A polymorphism at amino acid 1367 Cys (TTG)/Arg (CTG) reportedly reduces the risk of myocardial infarction in Japanese. We studied the possible involvement of this polymorphism in type 2 diabetes. When polymorphism of the *WRN* gene was analyzed in 272 randomly recruited type 2 diabetic subjects (age 64.5 ± 11.1), we found those with Cys/Arg to be older than those with Cys/Cys ($p = 0.021$) and that the age at diagnosis of diabetes was greater in Cys/Arg than in Cys/Cys subjects ($p = 0.011$). Diabetes-free survival rate over the age, analyzed by Kaplan–Meier method, differed significantly between these two genotype groups ($p = 0.0125$) and the survival curve was shifted to the right in the Cys/Arg group as compared to the Cys/Cys group. No difference in allele frequency was observed between our diabetic ($n = 272$) and non-diabetic subjects ($n = 171$, age 66.0 ± 8.0). These results suggest that the 1367 Arg allele of the *WRN* gene protects against the development of type 2 diabetes mellitus in Japanese.

Keywords: Type 2 diabetes mellitus; Werner's syndrome; *WRN* gene; *WRN* 1367 Cys/Arg polymorphism; Japanese

1. Introduction

Werner's syndrome is an autosomal recessive disease characterized by early onset of age-related diseases including cataracts, atherosclerosis, osteoporosis, and type 2 diabetes mellitus (DM) [1,2]. Positional cloning identified the gene responsible for Werner's syndrome, which was designated *WRN* [3]. *WRN* encodes a protein (WRN) that is a DNA helicase homologous to *E. coli* RecQ. WRN dysfunction is thought to result in DNA repair failure and acceleration of aging. Homozygous *WRN* mutations resulting in truncation of the protein were demonstrated in Werner's syndrome [4]. However, the effects of heterozygous mutations and rather minor genetic variations in *WRN* on common age-related diseases

* Corresponding author. Tel.: +81 22 717 7611; fax: +81 22 717 7612.
E-mail address: mhirai@int3.med.tohoku.ac.jp (M. Hirai).

0168-8227/$ – see front matter © 2005 Elsevier Ireland Ltd. All rights reserved.
doi:10.1016/j.diabres.2005.01.012

have not been clarified. A polymorphism at amino acid 1367 Cys (TTG)/Arg (CTG) of *WRN* is reportedly associated with myocardial infarction [5–7]; the 1367 Arg allele was suggested to play a protective role. In addition, heterozygous mutation is thought to be involved in common age-related disorders via its effects on the aging process [8]. However, the relevance of heterozygous mutations and the 1367 Cys/Arg polymorphism in type 2 diabetes mellitus has not been clarified. Herein we have shown, for the first time, that in randomly recruited diabetic subjects the development of diabetes is delayed in those with the 1367 Arg allele as compared to those without it. These results suggest that the 1367 Arg allele protects against the development of type 2 diabetes mellitus in Japanese.

2. Subjects and methods

2.1. Subjects

Two hundred and seventy two subjects with type 2 diabetes mellitus (male/female: 124/148) were randomly recruited from among patients seen in Tohoku University Hospital. Diabetes was diagnosed according to World Health Organization (WHO) criteria [9]. Subjects who had developed diabetes before age 30 were excluded from this study, since they may have had MODY or some other specific forms of diabetes. The clinical characteristics of all 272 diabetic subjects are shown in the left column of Table 1. Age at the time of this study averaged 64.5 ± 11.1, at diagnosis 48.8 ± 10.5. The age at diagnosis was determined based on medical records. Treatments were diet alone in 47, oral agents in 85 and insulin in 140. We also recruited 171 non-diabetic individuals as control subjects. The controls met one of the following sets of criteria: (1) age more than 50 and normal glucose tolerance by 75 g oral glucose tolerance test (OGTT) (86 subjects) or (2) HbA1c less than 5.6% and age 65 or older (85 subjects). Homeostasis model assessment for insulin resistance (HOMA-R) was calculated using the formula: fasting serum insulin (μU/ml) × fasting plasma glucose (mg/dl)/405. The study protocol was approved by the Tohoku University Institutional Review Board. Informed consent was obtained from all participants.

2.2. Genotype determination by the TaqMan polymerase chain reaction method

The *WRN* gene polymorphism (1367 Cys (TTG)/Arg (CTG)) was determined by the TaqMan probe method. Two dye-labeled probes were used in this allelic discrimination assay, one probe for each allele in the two-allele system. Each probe consists of an oligonucleotide with a 5′-reporter dye and a 3′-quencher dye. FAM (6-carboxy-fluorescein) was

Table 1
Clinical characteristics of all 272 diabetic subjects and their subgroups based on *WRN* 1367 Cys/Arg genotypes

	DM total	*WRN* 1367 genotype in DM		*p*
		Cys/Cys	Cys/Arg	
N (M/F)	272 (124/148)	244 (112/132)	28 (12/16)	0.759[a]
Age (years)	64.5 ± 11.1	63.9 ± 11.1	69.1 ± 10.1	0.021[b]
Age at diagnosis (years)	48.6 ± 10.5	48.0 ± 10.2	53.3 ± 11.8	0.011[b]
Diabetes duration (years)	15.9 ± 9.9	15.9 ± 9.8	15.8 ± 11.5	0.934[b]
BMI (kg/m^2)	23.5 ± 3.5	23.5 ± 3.4	23.6 ± 4.1	0.848[b]
Fasting plasma glucose (mg/dl)	135.3 ± 26.2	135.9 ± 26.8	130.5 ± 20.0	0.277[b]
HbA1c (%)	6.78 ± 1.10	6.82 ± 1.11	6.45 ± 0.91	0.085[b]
Therapy				
Diet	47 (17.3%)	40 (16.4%)	7 (25%)	0.107[a]
Oral agent	85 (31.3%)	81 (33.2%)	4 (14.3%)	
Insulin	140 (51.5%)	123 (50.4%)	17 (60.7%)	

Data are means ± S.D. unless otherwise specified. *p*-values were obtained by comparing the two genotype groups. DM: diabetes mellitus.
[a] Chi square test.
[b] Student's *t*-test.

covalently linked to the 5′-end of the probe for detection of the T allele. TET (tetrachloro-6-carboxy-fluorescein) was covalently linked to the 5′-end of the probe for detection of the C allele. Each of the reporters is quenched by TAMRA (6-carboxyl-*N,N,N′,N′*-tetramethylrhodamine) attached via a linker arm located at the 3′-end of each probe. The probes used in this study were as follows: a T allele-specific probe, 5′-Fam-CTT CAA CCT TCA TGT GAT GTC AAC AA-Tamra-3′, and a C allele-specific probe, 5′-Tet-CTT CAA CCT TCA CGT GAT GTC AAC AA-Tamra-3′. Primers designed for PCR in the flanking region of the C/T polymorphism in *WRN* were: forward, 5′-GCC TAA TCA GAA TGT TAG TTC C-3′; reverse, 5′-CCT CAG TAT TGA TGC CTA CTT C-3′. PCR was performed with PCR7700 (Applied Biosystems, USA). The fluorescence levels of PCR products were also measured using PCR7700.

2.3. Statistical analysis

Frequency analysis was performed with the chi square test. Significance of differences between group means was tested by Student's *t*-test or analysis of covariance (ANCOVA). Diabetes-free survival rate over the age was determined using Kaplan–Meier analysis and the log rank test in subject groups with the 1367 Cys/Arg or the 1367 Cys/Cys genotype. A *p*-value of less than 0.05 was considered statistically significant.

3. Results

Among 272 subjects with type 2 diabetes, 244 (89.7%) had the Cys/Cys genotype and 28 (10.3%) had the Cys/Arg genotype (Table 2). No subjects had Arg/Arg alleles. The genotype distribution in diabetic subjects did not deviate from Hardy–Weinberg equilibrium. Subjects with the Cys/Cys genotype were compared to those with the Cys/Arg genotype. The clinical characteristics of the diabetic subjects according to *WRN* 1367 genotypes are presented in Table 1. Interestingly, age at the time of the study was significantly greater in those with the Cys/Arg genotype (69.1 ± 10.1) than in those with the Cys/Cys genotype (63.9 ± 11.1) ($p < 0.021$). In addition, age at diabetes diagnosis was approximately 5 years greater in subjects with the Cys/Arg genotype (53.3 ± 11.8) than in those with the Cys/Cys genotype (48.0 ± 10.2) ($p < 0.011$).

Table 2
The Cys/Arg genotype distribution and allele frequencies in Japanese type 2 diabetic and non-diabetic control subjects

	DM	Control
n	272	171
Genotype distribution		
Cys/Cys	244 (89.7)	150 (87.7)
Cys/Arg	28 (10.3)	20 (11.7)
Arg/Arg	0 (0)	1 (0.6)
Cys/Arg + Arg/Arg	28 (10.3)	21 (12.3)
Chi square[a]	0.421	
Odds ratio[a]	1.22	
p[a]	0.51	
Allele frequency		
Cys	516 (94.9)	320 (93.6)
Arg	28 (5.1)	22 (6.4)
Chi square	0.65	
Odds ratio	1.27	
p	0.42	

Data are *n* (%), unless otherwise specified. DM: diabetes mellitus.
[a] Comparison between Cys/Cys and Cys/Arg + Arg/Arg.

Consistent with the age at diagnosis of diabetes differing between the two groups, diabetes-free survival rate over the age, depicted by the Kaplan–Meier method, clearly differed ($p = 0.0125$); the diabetes-free survival curve was shifted to the right in the Cys/Arg group as compared to the Cys/Cys group throughout the 30–80 age range (Fig. 1). The proportions of subjects who had become diabetic by age 50 were 50.0% and 60.7% in the Cys/Arg and the Cys/Cys groups, respectively. Similarly, the proportion who were diabetic by age 60, was also greater in the Cys/Cys (86.9%) than in the Cys/Arg (71.4%) group. Other clinical characteristics, such as BMI at the time of the study, did not differ between the two groups.

Among the 171 non-diabetic subjects, 150 (87.7%) were homozygous for the 1367 Cys allele, 20 (11.7%) were heterozygous and one (0.6%) was homozygous for the 1367 Arg allele. There was no deviation from Hardy-Weinberg equilibrium in control subjects. The genotype distribution did not differ significantly between diabetic and non-diabetic subjects (Table 2). The allele frequencies of the Cys allele

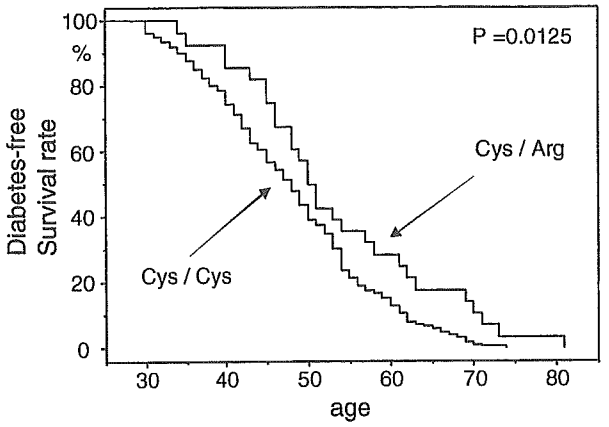

Fig. 1. Diabetes-free survival rate over the age according to the *WRN* 1367 Cys/Arg polymorphism in the diabetic subjects. Kaplan–Meier method.

and the Arg allele were 94.9% and 5.1%, respectively, in diabetic subjects and 93.6% and 6.4%, respectively, in control subjects. There was no statistically significant difference in allele frequencies between these groups.

Eighty-six out of 171 control subjects underwent OGTT to confirm their normal glucose tolerance, and plasma glucose and insulin levels in fasted and glucose challenged states were measured. Therefore, we analyzed the metabolic phenotypes of these subjects in more detail. The fasting glucose, 2 h glucose, fasting insulin, and 2 h insulin levels did not differ markedly (Table 3). Furthermore, HOMA-R (the index of insulin resistance) did not differ before ($p = 0.503$) and after ($p = 0.532$) adjustment for age, gender and BMI.

4. Discussion

Aging has a major influence on glucose intolerance. Werner's syndrome is highly associated with age-related diseases including cataracts, atherosclerosis, osteoporosis, and type 2 diabetes mellitus [1,2]. Thus, *WRN* is a reasonable candidate gene for type 2 diabetes mellitus susceptibility. Herein, we found the current age of diabetic patients with the 1367 Arg allele to be greater than that of those without this allele. In addition, subjects with the 1367 Arg allele develop diabetes later in life than those without this allele. These results suggest that the 1367 Arg allele plays a protective role against the development of diabetes mellitus. Our results might be suggested to simply reflect subjects with the Cys/Cys genotype dying at a younger age, regardless of diabetes. However, this is not the case. The current age of control subjects did not differ between those with (64.4 ± 9.3) and those without (66.2 ± 8.8) the Arg allele. This result may support the notion that subjects without the 1367 Arg allele are more likely to develop diabetes at a younger age than those with this allele, and younger patients are therefore more likely to be recruited into the Cys/Cys group. The following consideration should be reminded in the interpretation of the present results. In this study, we employed the age at diagnosis according to medical records rather than the age at diabetes onset, because it is nearly impossible to ascertain the exact onset of type 2 diabetes in this type of cross-sectional study. Diagnosis of diabetes at a clinical visit may reflect

Table 3
Clinical characteristics according to *WRN* 1367 Cys/Arg genotypes in the control subjects who underwent oral glucose tolerance test

	WRN 1367 genotype in control subjects with OGTT		*p*
	Cys/Cys	Cys/Arg	
N (M/F)	75 (47/28)	11 (9/2)	0.213[a]
Age (years)	59.8 ± 3.5	58.5 ± 2.9	0.232[b]
BMI (kg/m^2)	23.7 ± 2.6	23.2 ± 2.2	0.539[b]
Fasting plasma glucose (mg/dl)	90.7 ± 7.2	91.3 ± 8.0	0.801[b]
2 h plasma glucose (mg/dl)	105.1 ± 19.8	105.6 ± 27.4	0.934[b]
Fasting plasma insulin (μU/ml)	4.36 ± 2.76 ($n = 72$)	3.76 ± 1.89	0.492[b]
2 h plasma insulin (μU/ml)	27.55 ± 19.09 ($n = 71$)	27.61 ± 18.84 ($n = 9$)	0.993[b]
HOMA-R	0.99 ± 0.66 ($n = 72$)	0.85 ± 0.45	0.503[b]

Data are means ± S.D. *p*-values were obtained by comparing the two genotype groups. As complete clinical data were not available for all study subjects, the number of individuals is given in parentheses. OGTT: oral glucose tolerance test.

[a] Chi square test.

[b] Student's *t*-test.

the manifestation of diabetes related symptoms, thus the association of age at diagnosis with *WRN* genotype suggests that this polymorphism influences diabetes development.

Allele frequencies of this polymorphism do not differ between diabetic and non-diabetic subjects. It could be argued that these results are inconsistent with the notion that the 1367 Arg allele protects against the development of diabetes mellitus, as one would expect a higher frequency of the 1367 Arg allele in non-diabetic than in diabetic subjects. This argument is theoretically plausible. However, considering that only a fraction of the general population becomes diabetic and that the effect of the polymorphism is only to delay the onset of diabetes, the allele frequency difference between the diabetic and non-diabetic groups would presumably be very small. Our sample size was large enough to yield 80% power to detect a 5% deviation in the allele frequency between diabetic and control subjects (i.e. 5% in one group and 10% in the other) at a significance level of 0.05. However, the difference in the allele frequency was found to be smaller (5.1% versus 6.4%). Therefore, our results do not rule out the possibility of a slight but significant difference in allele frequency between the two groups, which could not be detected with a sample of this size.

One would expect non-diabetic subjects with the Arg 1367 allele to have slightly lower plasma glucose levels, but this was not the case. All clinical parameters measured, including fasting plasma glucose levels, were the same in subjects with the 1367 Cys allele and those with the 1367 Arg allele. Furthermore, although Werner's syndrome is characterized by insulin resistance, there was no evidence that the *WRN* 1367 polymorphism affected insulin sensitivity judging from the HOMA-R index data (Table 3).

The molecular basis of this polymorphism's contribution to the altered function of the WRN protein has yet to be fully defined. However, sequence analysis and studies using recombinant WRN protein and cells from Werner's syndrome patients have provided interesting findings. The 1367 Cys/Arg polymorphism is located three amino acids from the nuclear localization signal which contains multiple Arg and Lys residues [10,11]. An additional Arg residue near this domain could therefore enhance the rate of intracellular translocation towards the nucleus, thereby enhancing DNA repair capacity. DNA damage occurs with aging and may disturb many physiological functions including glucose metabolism. It is possible that subjects with the 1367 Arg allele are resistant to DNA damage and thus resistant to age-associated glucose intolerance. Further studies are needed to elucidate the roles of the 1367 polymorphism of *WRN* in the aging process and glucose metabolism.

In conclusion, the gene responsible for Werner's syndrome is also involved in the development of a common age-related disorder, diabetes mellitus. Furthermore, the 1367 Arg allele of this gene protects against the development of type 2 diabetes mellitus, delaying diabetes onset in Japanese subjects.

Acknowledgments

This work was supported by a Grant-in-Aid for Scientific Research on Priority Areas (C) "Medical Genome Science" (13204062 to Y.O.) and a Grant-in-Aid for Scientific Research (C) (14571082 to M.H.) from the Ministry of Education, Culture, Sports, Science and Technology of Japan.

References

[1] C.J. Epstein, G.M. Martin, A.L. Schultz, A.G. Motulsky, Werner's syndrome: a review of its symptomatology, natural history, pathologic features, genetics and relationships to the natural aging process, Medicine 45 (1996) 172–221.

[2] M. Goto, Hierarchical deterioration of body systems in Werner's syndrome: implications for normal aging, Mech. Ageing Dev. 98 (1997) 239–254.

[3] C.E. Yu, J. Oshima, Y.H. Fu, E.M. Wijsman, F. Hisama, R. Alisch, et al. Positional cloning of the Werner's syndrome gene, Science 272 (1996) 258–262.

[4] T. Matsumoto, O. Imamura, Y. Yamabe, J. Kuromitsu, Y. Tokutake, A. Shimamoto, et al. Mutation and haplotype analyses of the Werner's syndrome gene based on its genomic structure: genetic epidemiology in the Japanese population, Hum. Genet. 100 (1997) 123–130.

[5] L. Ye, T. Miki, J. Nakura, J. Oshima, K. Kamino, H. Rakugi, et al. Association of a polymorphic variant of the Werner helicase gene with myocardial infarction in a Japanese population, Am. J. Med. Genet. 68 (1997) 494–498.

[6] H. Morita, H. Kurihara, T. Sugiyama, C. Hamada, Y. Yazaki, A polymorphic variant $C^{1367}R$ of the Werner helicase gene and atherosclerotic diseases in the Japanese population, Thromb. Haemost. 82 (1999) 160–161.

[7] E. Castro, S.D. Edland, L. Lee, C.E. Ogburn, S.S. Deeb, G. Grown, et al. Polymorphisms at the Werner locus: II. 1074 Leu/Phe, 1367 Cys/Arg, longevity, and atherosclerosis, Am. J. Med. Genet. 95 (2000) 374–380.
[8] M. Satoh, M. Imai, M. Sugimoto, M. Goto, Y. Furuichi, Prevalence of Werner's syndrome heterozygotes in Japan, Lancet 353 (1999) 1766.
[9] K.G.M.M. Alberti, P.Z. Zimmet, Definition, diagnosis and classification of diabetes mellitus and its complications part 1: Diagnosis and classification of diabetes mellitus. Provisional report of a WHO consultation, Diabet. Med. 15 (1998) 539–553.
[10] T. Matsumoto, A. Shimamoto, M. Goto, Y. Furuichi, Impaired nuclear localization of defective DNA helicases in Werner's syndrome, Nat. Genet. 16 (1997) 335–336.
[11] T. Matsumoto, O. Imamura, M. Goto, Y. Furuichi, Characterization of the nuclear localization signal in the DNA helicase involved in Werner's syndrome, Int. J. Mol. Med. 1 (1998) 71–76.

THE JOURNAL OF BIOLOGICAL CHEMISTRY VOL. 280, NO. 51, pp. 42016–42025, December 23, 2005

Resistin-like Molecule β Activates MAPKs, Suppresses Insulin Signaling in Hepatocytes, and Induces Diabetes, Hyperlipidemia, and Fatty Liver in Transgenic Mice on a High Fat Diet*

Received for publication, March 21, 2005, and in revised form, October 18, 2005 Published, JBC Papers in Press, October 21, 2005, DOI 10.1074/jbc.M503065200

Akifumi Kushiyama[‡], Nobuhiro Shojima[‡], Takehide Ogihara[§], Kouichi Inukai[¶], Hideyuki Sakoda[‡], Midori Fujishiro[‡], Yasushi Fukushima[‡], Motonobu Anai[‖], Hiraku Ono[‖], Nanao Horike[**], Amelia Y. I. Viana[**], Yasunobu Uchijima[**], Koichi Nishiyama[**], Tatsuo Shimosawa[‡], Toshiro Fujita[‡], Hideki Katagiri[§], Yoshitomo Oka[§], Hiroki Kurihara[**], and Tomoichiro Asano[1]**

From the [‡]Department of Internal Medicine, Graduate School of Medicine, University of Tokyo, 7-3-1 Hongo, Bunkyo-ku, Tokyo 113-8655, the [§]Division of Advanced Therapeutics for Metabolic Diseases, Center for Translational and Advanced Animal Research on Human Diseases, Tohoku University Graduate School of Medicine, 1-1 Seiryo-machi, Sendai, Miyagi 980-8574, the [¶]Division of Endocrinology and Diabetes, Department of Medicine, Saitama Medical School, Morohongo 38, Moroyama, Iruma-gun, Saitama 350-0495, the [‖]Department of Internal Medicine, Institute for Adult Diseases, Asahi Life Foundation, 1-6-1, Marunouchi, Chiyoda-ku, Tokyo 100-0005, and the [**]Department of Physiological Chemistry and Metabolism, Graduate School of Medicine, University of Tokyo, 7-3-1 Hongo, Bunkyo-ku, Tokyo 113-8655, Japan

Resistin and resistin-like molecules (RELMs) are a family of proteins reportedly related to insulin resistance and inflammation. Because the serum concentration and intestinal expression level of RELMβ were elevated in insulin-resistant rodent models, in this study we investigated the effect of RELMβ on insulin signaling and metabolism using transgenic mice and primary cultured hepatocytes. First, transgenic mice with hepatic RELMβ overexpression were shown to exhibit significant hyperglycemia, hyperlipidemia, fatty liver, and pancreatic islet enlargement when fed a high fat diet. Hyperinsulinemic glucose clamp showed a decreased glucose infusion rate due to increased hepatic glucose production. In addition, the expression levels of IRS-1 and IRS-2 proteins as well as the degrees of insulin-induced phosphatidylinositol 3-kinase and Akt activations were attenuated in RELMβ transgenic mice. Similar down-regulations of IRS-1 and IRS-2 proteins were observed in primary cultured hepatocytes chronically treated (for 24 h) with RELMβ, suggesting the insulin resistance-inducing effect of RELMβ to be direct. Furthermore, it was shown that RELMβ acutely and markedly activates ERK and p38, while weakly activating JNK, in primary cultured hepatocytes. This increased basal p38 phosphorylation level was also observed in the livers of RELMβ transgenic mice. In conclusion, RELMβ, a gut-derived hormone, impairs insulin signaling probably via the activations of classic MAPKs, and increased expression of RELMβ may be involved in the pathogenesis of glucose intolerance and hyperlipidemia in some insulin-resistant models. Thus, RELMβ is a potentially useful marker for assessing insulin resistance and may also be a target for future novel anti-diabetic agents.

Insulin resistance is a major cause of type 2 diabetes, and recent studies have revealed many independent mechanisms regulating insulin sensitivity. Among them, much attention has been paid to the roles of secreted proteins in insulin resistance. Resistin (also known as FIZZ3 ADSF, mXCP4, or hXCP1) was identified as a factor that is secreted by adipocytes and causes insulin resistance (1). This finding was supported by not only *in vitro* experiments using cultured cells but also animal experiments, *i.e.* mice with adenoviral resistin expression, infusion of recombinant resistin, the use of neutralizing antibody, or by generating resistin gene knock-out mice (2–6). However, some clinical studies have failed to demonstrate a close relationship between obesity or insulin resistance and the serum resistin concentration in humans (7, 8). Thus, while resistin apparently induces insulin resistance, the involvement of resistin in the pathogenesis of human diabetes and obesity remains unclear.

On the other hand, there are three resistin-related proteins, termed RELMα[2] (resistin-like molecule, FIZZ1, or mXCP2), β (FIZZ2, mXCP3, or hXCP2), and γ (mXCP1) (9). RELMα is expressed in white adipose tissue, the lung, tongue and bone marrow, whereas the expression of RELMβ is strictly limited to the small and large intestines, especially goblet cells. Although RELMγ is expressed in mouse spleen, bone marrow, intestines, and a variety of other tissues, corresponding to each developmental stage depending on CAAT/enhancer-binding protein-ϵ (10), its human homolog has not been identified. These proteins contain a highly conserved cysteine-rich C terminus (Cys-X_{11}-Cys-X_8-Cys-X-Cys-X_2-Cys-X_{10}-Cys-X-Cys-X-Cys-X_9-Cys-Cys) and a signal peptide sequence at their N termini, as observed in resistin. Assuming that they have biological activities similar to that of resistin, these RELMs and resistin are considered to be equally important for the regulation of insulin sensitivity. Indeed, it was reported that injecting mice with either resistin or RELMβ induced insulin resistance (11). In addition, we found the intestinal expression and serum concentration of RELMβ to be increased in insulin resistant models such as high fat fed and *db/db* mice (12). Thus, we speculated that the inflammatory state of the intestine, overeating, bowel movements, and/or nutrient absorption might regulate the intestinal expression and serum level of RELMβ and thereby regulate whole-body insulin sensitivity.

* The costs of publication of this article were defrayed in part by the payment of page charges. This article must therefore be hereby marked "*advertisement*" in accordance with 18 U.S.C. Section 1734 solely to indicate this fact.

[1] To whom correspondence should be addressed. Tel.: 81-3-5841-3603; Fax: 81-3-5803-1874; E-mail: asano-tky@umin.ac.jp.

[2] The abbreviations used are: RELM, resistin-like molecule; MAPK, mitogen-activate protein kinase; IRS, insulin receptor substrate; SAPK, stress-activated protein kinase; JNK, c-Jun N-terminal kinase; 2DG, 2-deoxy-D-glucose; PI, phosphatidylinositol; SAP, serum amyloid P; PPARα, peroxisome proliferator-activated receptor α.

Herein, to examine chronic effects of the elevated serum RELMβ observed under insulin-resistant conditions such as a high fat diet and in *db/db* mice, we generated transgenic mice overexpressing RELMβ and analyzed their metabolic profiles relating to insulin resistance and changes in the insulin signaling pathway. Furthermore, to investigate the physiological significance of elevated serum RELMβ, we investigated the effects of RELMβ on insulin signaling using primary cultured hepatocytes. Herein, we show that RELMβ activates three MAPKs and down-regulates IRS-1/2 proteins and suppresses insulin signaling. Our observations suggest that RELMβ may be a useful marker for assessing insulin resistance associated with obesity and may also serve as a target for future novel anti-diabetic agents.

MATERIALS AND METHODS

Antibodies—The affinity-purified antibodies against RELMβ, insulin receptor substrate (IRS)-1, IRS-2, tyrosine phosphorylation (4G10), and Akt/protein kinase B were prepared as previously described (13). The antibodies against phospho-Ser473 of Akt, phospho-p44/p42, p44/42, phospho-p38 MAPK, p38 MAPK, phospho-SAPK/JNK, and SAPK/JNK were purchased from Cell Signaling Technology.

Preparation of Recombinant RELMβ—Adenoviruses expressing RELMβ were constructed using an Ad Easy kit (Quantum Biotechnology). HEK293 T cells transfected with RELMβ adenovirus produced 50–100 mg/liter RELMβ protein in the medium. Serum-free medium CD293 (Invitrogen) was used to collect the secreted protein from confluent HEK293 T cells for 2 days. The medium was harvested and spun down to remove cells. The medium was then purified and concentrated using a high S column and Biologic LP system (Bio-Rad) as described previously (4). Greater than 95% purity was confirmed by silver staining with a Silver Staining Kit (BEXEL Biotechnology), and quantities were determined by Western blotting, using commercially available recombinant RELMβ (Peprotech) as the standard. The medium of HEK293T cells transfected with β-galactosidase expressing adenovirus was used to prepare a control solution. The pH values of RELMβ and control solution were adjusted to 7.4.

Construction of RELMβ and Generation of Transgenic Mice—The open reading frame of RELMβ was obtained employing PCR based on the previously reported sequence (9). This RELMβ cDNA was cloned into a pAT15-3 vector containing the SAP promoter and rat β-globin intron (Fig. 1*a*), which was used for the generation of RELMβ transgenic mice.

Animals and High Fat Diet—The C57/Bl6 line was used to generate RELMβ transgenic mice. All animal studies were conducted according to the Japanese guidelines for the care and use of experimental animals. All animal experiments were performed after 4-week high fat diet loading, unless otherwise indicated. The high fat diet had, basically, the previously described composition (14), except that the skim was added to the formulation. Food intakes were determined daily for 5 consecutive days. Food was withdrawn 12 h before each experiment.

Immunoblotting of RELMβ—Serum RELMβ concentrations in transgenic mice and their littermates were determined by immunoblotting. Two microliters of serum was boiled in Laemmli sample buffer containing 100 mM dithiothreitol. Samples were subjected to SDS-PAGE, transferred to 0.1-μm pore nitrocellulose, and immunoblotted using anti-RELMβ antibody (1:1000). Proteins were visualized with enhanced chemiluminescence (ECL or ECL plus) and exposed to ECL film (Amersham Biosciences)

Serum Glucose, Lipids, and Hepatic Triglyceride and Glycogen—Blood glucose was measured with a portable blood glucose monitor, Freestyle Kissei (Kissei Pharmaceutical, Japan). The plasma insulin level was determined with an enzymatic immunoassay kit (Amersham Biosciences). Serum triglyceride, cholesterol, and free fatty acids were assayed with Triglyceride E test Wako, Cholesterol E test Wako, and NEFA C test Wako (Wako Chemicals, Japan), respectively. Serum adiponectin was assayed with an adiponectin measurement kit (Otsuka Pharmaceuticals, Japan). Hepatic total lipid was extracted and assayed using the Folch method, as described previously (15). The triglyceride content was assayed as described above. Hepatic glycogen content was measured as previously described (16).

Tolerance Test—Glucose (2 g/kg glucose load), insulin (0.75 unit/kg insulin), and pyruvate (2 g/kg pyruvate) tolerance tests were performed as previously described (17).

Glucose Clamp Study—The glucose clamp study was performed, as previously described (18–21), with some modifications. In brief, mice were implanted with catheters that were exteriorized at the back of the neck and encased in silastic tubing. Four days after surgery, the animals were fasted for 3 h and used for the experiments. [D-^{3}H]Glucose (Amersham Biosciences) was injected (bolus 10 μCi, 0.1 μCi/min, for 240 min) intravenously. After a 90-min basal period, a blood sample was collected for determination of glucose-specific activity and the blood glucose level. At time 0, hyperinsulinemic-euglycemic clamps were started, and 10 milliunits/kg/min human insulin (Novolin R, Novo Nordisk) was continuously infused for 150 min. The blood glucose concentration was clamped at 90–120 mg/dl, for at least 60 min, by estimating the blood glucose concentration at 5-min intervals and adjusting the rate of glucose solution infusion. Blood samples were taken to determine blood glucose, insulin, and plasma [D-^{3}H]glucose every 30 min for 120 min. Then, 12 μCi of [^{14}C]2-deoxy-D-glucose ([^{14}C]2DG, Amersham Biosciences) was injected, and blood samples were taken at 122, 125, 130, and 150 min to determine blood glucose and plasma [^{14}C]2DG. At 150 min, the gastrocnemius (type IIB fibers) muscle, soleus (type I and type IIA fibers) muscles, and epididymal fat were immediately excised and frozen in liquid nitrogen, then stored at −80 °C until future tissue analysis.

Plasma and Tissue Assays in Glucose Clamp Study—After deproteinization with barium hydroxide ($Ba(OH)_2$, 0.3 N) and zinc sulfate ($ZnSO_4$, 0.3 N), [D-^{3}H]glucose and [^{14}C]2DG radioactivities of plasma were determined by dual channeled liquid scintillation counting. Hepatic glucose production and the glucose disposal rate were calculated for the basal period and the steady-state portion of the glucose clamp as previously described (21). Muscle and fat samples were weighed and homogenized in 0.5% perchloric acid. Homogenates were centrifuged and neutralized with $NaHCO_3$. The sample was then separated into two aliquots. One was counted directly to determine [^{14}C]2DG and [^{14}C]2DG-6-phosphate ([^{14}C]2DGP) radioactivities. The other was treated with $Ba(OH)_2$ and $ZnSO_4$ to remove [^{14}C]2DGP and any tracer incorporated into glycogen and then counted to determine [^{14}C]2DG radioactivity. [^{14}C]2DGP is the difference between the two aliquots. Tissue glucose uptake was calculated as described (20).

In Vivo Insulin Stimulation—In vivo insulin stimulation was performed, as previously described (22), with some modifications. In brief, mice were anesthetized with pentobarbital sodium. The portal vein was exposed, and 0.4 ml of normal saline (0.9% NaCl) with or without insulin (25 milliunits/g body wt) was injected. The livers were removed 30 s later, and hind limb skeletal muscles were removed 90 s thereafter and immediately homogenized with a Polytron homogenizer in 6 volumes of solubilization buffer. Both extracts were centrifuged at 15,000 × *g* for 30 min at 4 °C, and the supernatants were used as samples for immunoprecipitation, immunoblotting, or kinase assay of PI 3-kinase and Akt/protein kinase B.

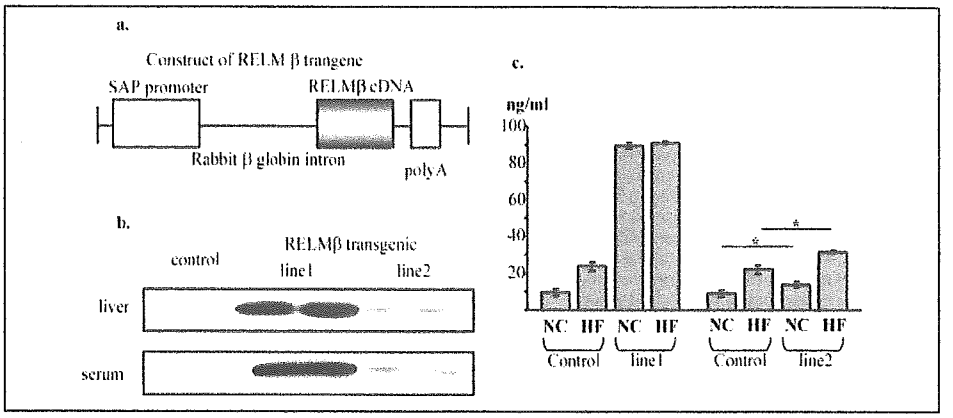

FIGURE 1. *a*, schematic drawing of the construct for RELMβ gene overexpression. *b*, hepatic expressions and elevated serum concentrations of RELMβ in the two lines of RELMβ transgenic mice. Immunoblotting revealed line 1 and line 2 transgenic mice to have high and low levels of RELMβ overexpression, respectively. *c*, quantification using recombinant RELMβ as the standard. Western blotting was performed by transferring samples, using standards for the same membrane. Values are presented as means ± S.E. In line 2 mice, statistical significance is indicated by an *asterisk*: *, $p < 0.05$ for RELMβ transgenic mice *versus* control age-matched mice. *NC*, normal chow; *HF*, high fat.

Immunoprecipitation and Immunoblotting—Supernatants containing equal amounts of protein (8 mg) were incubated with anti-IRS-1 and anti-IRS-2 antibodies (5 mg/ml each) and then incubated with 100 μl of protein A- and G-Sepharose. The samples were washed and then boiled in Laemmli sample buffer containing 100 mM dithiothreitol. Total lysates were also boiled to allow detection of Akt, AktSer473 phosphorylation, the three MAPKs, and their phosphorylations. Total lysates or immunoprecipitants were subjected to Western blotting, blotted with one of the antibodies or 4G10 antibody. Band intensities were quantified with Image J (National Institutes of Health).

Measurement of PI 3-Kinase and Akt/Protein Kinase B Activity—For PI 3-kinase assay, the supernatants containing equal amounts of protein were immunoprecipitated for 2 h at 4 °C with anti-IRS-1, anti-IRS-2 or 4G10 antibody and protein A- or G-Sepharose. PI 3-kinase activities in the immunoprecipitants were assayed as previously described (23). For the Akt kinase assay, an Akt kinase assay kit (Cell signaling) was used according to the manufacturer's instructions.

Glucose Uptake by Isolated Soleus Muscle in Vitro—Insulin-stimulated glucose uptake by the soleus muscle was measured as described previously (24). Mouse soleus muscles were isolated and incubated for 30 min in KHB buffer, with or without human insulin (2 milliunits/ml). The muscles were then rinsed for 10 min at 29 °C and incubated for 20 min at 29 °C in KHB buffer containing 8 mM 2-deoxy-D-[1,2-^{3}H]glucose (2-DG) (2.25 μCi/ml) and 32 mM [^{14}C]mannitol (0.3 μCi/ml). After incubation, the muscles were rapidly solubilized. Radioactivity in the resultant samples was counted, and 2-DG uptake rates were corrected for extracellular trapping with mannitol counts.

Effects of RELMβ on Insulin Action in Primary Hepatocytes—Hepatocytes were isolated from fasted C57/bl6 mice by collagenase perfusion, as described previously (25). To determine the effects of RELMβ on insulin signaling, the dishes were split into two groups corresponding the presence and absence of RELMβ stimulation for 24 h. The RELMβ concentration was 1 μg/ml. The cells were then serum-starved for 3 h and stimulated with 10^{-6} M insulin for 5 min at 37 °C. IRS-1 and IRS-2 protein contents were evaluated by immunoblotting as described above. Insulin-induced IRS-1 and IRS-2 phosphorylations were evaluated by 4G10 immunoprecipitation and immunoblotting as described above.

Effect of RELMβ on Phosphorylations of MAPKs—To determine the effects of RELMβ on MAPK phosphorylations with their time course and dose dependence, primary hepatocytes were stimulated with 1 μg/ml RELMβ for 10 or 30 min, and with 0.01, 0.1, or 1 μg/ml RELMβ for 15 min. Phosphorylations of p44/p42 (ERK1/2), p38 MAPK, and p54/p46 (SAPK/JNK) were evaluated by immunoblotting as described previously (26).

Tissue Hematoxylin-Eosin Staining—The liver and pancreas were removed from transgenic mice and their littermates and formalin-fixed. Samples were routinely embedded in paraffin. Approximately 5-μm-thick slices obtained from these samples were stained with hematoxylin and eosin. Mean pancreatic islet area was histomorphometrically analyzed as previously described (27), using ImageJ (National Institutes of Health).

Ribonuclease Protection Assay—Riboprobes of enzymes were amplified from mouse embryonic cDNA using PCR primers and subcloned as already described (13). Total RNA from the liver and primary cultured hepatocytes was isolated using TRIzol reagent (Isogen, Nippon Gene, Japan). A 10-μg RNA sample was used for each assay. RNase protection assays were carried out according to the manufacturer's instructions (RPA III kit, Ambion, Austin, TX). Intensities of the resultant bands were determined using BAS2000 (Fuji film, Japan).

Statistical Analysis—Results are expressed as means ± S.E., and significance was assessed using unpaired Student's *t* tests, unless otherwise indicated.

RESULTS

Generating RELMβ Transgenic Mice—We generated transgenic mice, the livers of which express RELMβ, by inserting RELMβ cDNA downstream from the serum amyloid P (SAP) promoter. As expected, liver-specific expression in these transgenic mice was confirmed (data not shown), and two lines were established. In the livers of line 1 mice, RELMβ was highly overexpressed, and the serum RELMβ concentration exceeded that of the non-transgenic mice by 10-fold (Fig. 1*c*). In line 2 mice, RELMβ was moderately overexpressed, and the resulting elevation of serum RELMβ was approximately double that in non-transgenic mice (Fig. 1*c*). Hepatic RELMβ expression was reportedly increased in response to high fat feeding. Thus, increases in serum RELMβ with a high fat diet were observed in wild-type and line 2 mice, whereas there was no marked increase in the line 1 mice in which hepatic RELMβ overexpression was high. These observations indicate that a high fat diet increases endogenous RELMβ expression but not transgene-derived RELMβ expression.

No significant difference was observed in terms of growth or adolescence between RELMβ transgenic mice and their littermates. At the time of sacrifice (age 16 weeks, after 4 weeks of being fed a high fat diet) and within the observation period, there was no significant difference in body weight or food intake.

Glucose and Lipid Metabolic Profiles of RELMβ Transgenic Mice—The body weight, fasting serum glucose, serum insulin, and lipid concentrations of RELMβ transgenic mice did not differ from those of control mice when both were fed normal chow, at the age of 16 weeks.

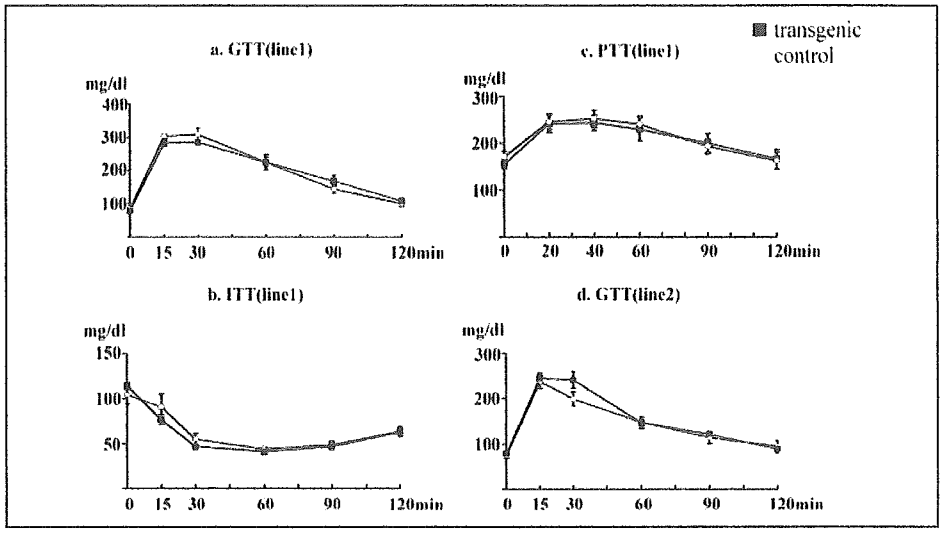

FIGURE 2. **Intraperitoneal glucose tolerance test (GTT), insulin tolerance test (ITT), and pyruvate tolerance test (PTT) in age-matched RELMβ transgenic (■, $n = 6$ for line 1 and $n = 5$ for line 2) and control mice (○, $n = 7$ for line 1 and $n = 8$ for line 2).** *a* and *d*, GTT for line 1 (age 6 weeks, normal chow) and 2 (age 6 weeks, normal chow) in comparison with the control mice. *b*, ITT for line 1 (age 7 weeks, normal chow) in comparison with the control mice. *c*, PTT for line 1 (age 8 weeks, normal chow) in comparison with the control mice. Values are presented as means ± S.E.

TABLE ONE

Glucose and lipid metabolic profiles of 16-week-old RELMβ transgenic mice on normal chow

Values are indicated as means ± S.E. *TC*, total cholesterol; *TG*, triglyceride.

	Control (line 1)	Transgenic (line 1)	Control (line 2)	Transgenic (line 2)
BW (g)	17.2 ± 0.8	17.9 ± 0.5	15.4 ± 1.1	16.4 ± 0.6
FBS (mg/dl)	88.9 ± 4.1	92.0 ± 2.4	81.2 ± 2.7	86.8 ± 2.6
Serum insulin (ng/ml)	0.08 ± 0.02	0.11 ± 0.02		
Serum TC (mg/dl)	38.2 ± 2.2	36.7 ± 3.3		
Serum TG (mg/dl)	49.6 ± 8.1	49.0 ± 5.8		
Serum free fatty acid (mEq/liter)	0.80 ± 0.08	0.63 ± 0.07		

TABLE TWO

Glucose and lipid metabolic profiles of RELMβ transgenic mice, at the age of 16 weeks, which had been fed a high fat diet for 4 weeks

Values are indicated as means ± S.E. *TC*, total cholesterol; *TG*, triglyceride.

	Control (line 1)	Transgenic (line 1)	Control (line 2)	Transgenic (line 2)
Body weight (g)	37.1 ± 2.6	36.5 ± 1.4	31.5 ± 1.5	33.9 ± 2.6
Food intake (g/day)	4.6 ± 0.4	4.5 ± 0.5	4.1 ± 0.2	4.3 ± 0.8
FBS (mg/dl)	109.5 ± 8.3	156.1 ± 10.6[a]	117.3 ± 3.9	132.0 ± 2.8[a]
Serum insulin (ng/ml)	3.8 ± 0.7	12.3 ± 2.7[a]	5.4 ± 1.3	7.6 ± 1.4
Serum TC (mg/dl)	48.0 ± 3.6	61.2 ± 7.9[a]	50.3 ± 4.5	76.4 ± 13.6
Serum TG (mg/dl)	51.7 ± 6.4	84.6 ± 6.4[a]	75.9 ± 8.0	103.3 ± 14.0[a]
Serum free fatty acid (mEq/l)	0.59 ± 0.02	0.56 ± 0.04	NT[b]	NT
Serum adiponectin (μg/ml)	14.1 ± 1.4	11.1 ± 0.9	NT	NT
Liver TG (mg/g liver)	14.3 ± 1.9	21.0 ± 2.9[a]	NT	NT
Liver glycogen (mg/g liver)	1.96 ± 0.08	1.97 ± 0.10	NT	NT
Islet area (μm^2)	36310 ± 6357	92760 ± 9571[a]	NT	NT

[a] Statistical significance: $p < 0.05$ for control mice *versus* transgenic mice.
[b] NT, not tested.

Furthermore, glucose, insulin, and pyruvate tolerance tests showed no significant differences between 16-week-old RELMβ-overexpressing mice and their littermates (Fig. 2, *a–d*, and TABLE ONE). However, the serum glucose concentration was significantly more elevated in both lines of transgenic mice ($n = 25$, $p < 0.01$) when fed a high fat diet (TABLE TWO), than those in the control mice. Under these conditions, hyperinsulinemia ($n = 6$, $p < 0.05$), hyperlipidemia ($n = 6$, $p < 0.05$), and increased hepatic triglyceride content ($n = 8$, $p < 0.05$) were observed in the transgenic mice.

Starting at the age of 16 weeks (line 1), or 20 weeks (line 2), mice were given a high fat diet for 4–6 weeks, and glucose, insulin, and pyruvate tolerance tests were then performed (Fig. 3). The glucose tolerance test confirmed an elevated fasting serum glucose concentration (Fig. 3, *a* and *d*) and revealed glucose intolerance in the transgenic mice. The insulin tolerance test revealed insulin resistance in the transgenic mice (Fig. 3, *b* and *e*). Finally, the pyruvate tolerance test showed greater elevation of the serum glucose concentration in the transgenic mice, as compared with the control mice (Fig. 3, *c* and *f*), indicating insufficient suppression of hepatic gluconeogenesis in the transgenic mice. Taking these results together, RELMβ transgenic mice are insulin-resistant and glucose-intolerant, particularly in the liver. These tendencies were more evident in the highly RELMβ-overexpressing line. In terms of adipocytokines,